Experimental investigation on the effects of bed slope and tailwater on dam-break flows

Wenjun Liu[1], Bo Wang[2], Yakun Guo[3], Jianmin Zhang[4], Yunliang Chen[5]

[1]PhD student, State Key Laboratory of Hydraulics and Mountain River Engineering, Sichuan University, Chengdu, 610065, China. E-mail: liuwenjun_scu@163.com

[2]Professor, State Key Laboratory of Hydraulics and Mountain River Engineering, Sichuan University, Chengdu, 610065, China. E-mail: wangbo@scu.edu.cn(Corresponding author)

[3]Professor, Faculty of Engineering & Informatics, University of Bradford, BD7 1DP, UK. E-mail: y.guo16@bradford.ac.uk

[4]Professor, State Key Laboratory of Hydraulics and Mountain River Engineering, Sichuan University, Chengdu, 610065, China. E-mail: zhangjianmin@scu.edu.cn

[5]Professor, State Key Laboratory of Hydraulics and Mountain River Engineering, Sichuan University, Chengdu, 610065, China. E-mail: 13541291332@163.com

Abstract: Understanding of the characteristics of dam-break flows moving along a sloping wet bed can help to timely issue flood warning and risk mitigation. In this study, laboratory experiments are carried out in a large flume for a wide range of upstream water depth, bed slopes and tailwater depth. The water level is recorded and processed to calculate the mean velocity and wave celerity. Results show that the increase of the bed slope will significantly accelerate the wave-front celerity for the downstream dry bed, while the negative wave celerity will decrease. When water depth ratio $\alpha \geq 0.3$ (defined as the ratio of initial downstream water depth over the upstream water depth of dam), there are extra negative waves propagating towards the reservoir area after the flow has developed for a period of time. When $\alpha \geq 0.6$, there are the Favre waves propagating downstream. The water level and the mean velocity fluctuate due to the influence of the extra negative waves and the Favre waves. Such fluctuant frequency increases with the increase of the water depth ratio. The empirical formulas are obtained for the celerity of the first extra negative wave and the first

downstream wave. The variation of wave-front height is very similar under three bed slopes investigated in this study, while the maximum wave-front height occurs when α = 0.2. The present study broadens the understanding of the effects of the bed slope and the tailwater level on the movement of the dam-break flows. Furthermore, experimental results are also compared with some analytical solutions. The validity of the assumptions made during the development of these analytical solutions and their limitations are discussed by comparing with the experimental measurements.

Keywords: Dam-break flow; Bed slope; Water depth ratio; Water level; Wave celerity; Digital image processing.

1. Introduction

The dam-break floods have significant destructive power, which can seriously threaten the lives and properties downstream of the dam (Plate, 2005; Hamlet and Lettenmaier, 2007; Wang et al., 2020a). It is, therefore, important to investigate the evolution characteristics of the dam-break flood in order to mitigate flood risk and reduce losses. Previous studies showed that the dam-break flow was affected by various factors (Miller and Chaudhry, 1989; Feizi et al., 2012; Van et al., 2014; Hooshyaripor and Tahershamsi, 2015; Wood and Wang, 2015; Juez et al. 2017; Wang et al., 2016, 2018). Among them, the bed slope and the downstream tailwater depth play important roles in the development of the dam-break flows. Knowledge and understanding of the propagation characteristics of the dam-break flow under the combined effect of the bed slope and the downstream tailwater depth can help issue timely flood warning and prepare appropriate mitigation measures.

Extensive studies have been carried out to investigate the effect of the bed slope on the evolution of the dam-break flow in past decades. Dressler (1958) used the form of the second type of elliptic integrals to derive the analytical solution of the dam-break flow under the condition of the dry sloped bed. Mungkasi and Roberts (2011) applied the method of characteristics to derive the

analytical solution in the case of the dry sloped bed. They developed the mathematical equation to describe the water surface profile. Chanson (2009) considered the role of the wave-front resistance, and used the similar method to derive the analytical solution for the dry sloped bed. In his solution, the water depth in the wave-front region was affected by the selection of the surface roughness height k_s. Wang et al. (2017) deduced the analytical solution of the dry sloped bed under arbitrary cross-sectional shape by using the method of cross-sectional shape parameter separation. Using different methods, various analytical solutions are also obtained (Fernandez-Feria, 2006; Mangeney et al. 2000; Wang and Pan, 2014). The studies discussed above mainly focused on the effect of bed slope on the dam break flow. However, the downstream water depth (i.e., tailwater depth) also affects the propagation of the dam break flow. The role of the tailwater was investigated by Hunt (1983) who applied the dynamic wave approximation method to derive the analytical solution of the dam-break flows along a wet sloped bed. However, this analytical solution was only accurate after the flow moved downstream for a certain distance which was affected by the upstream water depth. This restricts the application of this analytical solution. Mungkasi and Roberts (2012) adopt the solving method of Stoker's (1957) shock discontinuity, and used the method of characteristics to derive the analytical solution in the case of wet sloped bed. Wang et al. (2020b) also used a similar method to derive the analytical solution of shallow water equations along a wet sloped bed. However, these analytical solutions have not been systematically verified by experimental data, and their capability to describe the actual dam-break flow also remains to be studied.

The laboratory experiment is another method for investigating the dam-break flow (Denlinger and O'Connell, 2008; Cochard and Ancey, 2008; Marra et al., 2011, Wang et al., 2019). Lauber and Hager (1998b) carried out laboratory experiments in a smooth, rectangular prismatic flume with downstream dry bed to investigate the water surface profiles, flow velocity, negative wave and wave-front position. From their experiments, they proposed empirical formulas to describe the variation of these hydraulic parameters. Nsom et al. (2000) conducted the experiment in downstream

dry bed using the glucose syrup-water solutions. The dam-break flow propagation was measured and recorded by using image processing technology and ultrasonic distance detection system. The movement of the wave-front was analyzed and compared with the derived theoretical solution. The analysis of the hydraulic parameters, such as the flow velocity and the negative wave celerity, however, was not sufficient. Chen et al. (2014) studied the impact load on the downstream dam induced by the dam-break flows. Three typical impact modes were observed, and an empirical formula was proposed to describe the temporal variation of pressure load. However, the characteristic of dam-break flow was not analyzed. The above experimental studies have the characteristics of only considering the dry sloped bed, further experimental studies for the wet sloped bed case are required.

In addition, the sudden changes of the flow discharge may cause the periodic oscillations waves (Favre waves) to propagate through the channel. These waves may damage the structure in the channel, and also affect the operation of the channel and the navigation of the ships. Favre (1935) conducted a systematic experimental measurement of the propagation characteristics of these waves in a rectangular channel. Treske (1994) performed a similar study in rectangular and trapezoidal channels and found that the frequencies of secondary waves in the rectangular channel are higher than that in the trapezoidal channel for the same Froude numbers case. Peregrine (1966) invented a numerical model that can describe the propagation of an undular bore, but the model cannot be calculated from the initial discontinuous free surface. Soares-Frazao and Zech (2002) had improved the previous numerical model, and proposed a stable finite volume scheme that can be calculated from a steep front to compute secondary waves. However, previous studies on Favre waves rarely take into account the impact of the bed slope. What effect does the gravity component have on the conformation and propagation of Favre waves? What is the difference between the propagation characteristics of Favre waves on sloped channel and horizontal channel? To answer the above questions, further study should be carried out considering the bed slope.

There are little studies on the dam-break flows (or Favre waves) moving along the sloping wet bed, which is often encountered in the real situation. Therefore, the characteristic of the dam-break flows (or Favre waves) propagating along a sloping, initially wet bed has not been fully understood. In this paper, laboratory experiments are carried out in a large flume for a wide range of upstream water depth, bed slope and tailwater depth to investigate the propagation feature of the dam break flows (or Favre waves). The water level is recorded by CCD cameras and is then obtained by image processing technology. Mean velocity and wave celerity are then calculated. Results obtained from this study can be used as a reference for issuing the actual flood warning and mitigation work and also for validating the new analytical solution or numerical model.

2. Experimental setup

2.1. Water flume

The experiment is carried out at the State Key Laboratory of Hydraulics and Mountain River Engineering, Sichuan University, China. The flume has the dimension of 18 m in length, 1 m in width and 1.09 m in height. The flume is divided into two parts by using a 15 mm thick fiberglass board at 8.37 m from the inlet, while the downstream water level is adjusted by changing the blocking height of the rigid fiberboard, as shown in Fig. 1. In Fig. 1, h_u, h_d is the initial water depth of the upstream and downstream, respectively and S_0 is the bed slope. The flume is made of transparent tempered glass and supported by steel pillars whose height can be adjusted independently. The slope of the flume can be changed by adjusting the height of these pillars. The gate is connected to the motor through the steel cable. When the upstream water depth is 0.4 m, the corresponding lifting time is 0.167 s, which satisfies the transient collapse condition (Lauber and Hager, 1998a) $t < (2h_u/g)^{1/2} = 0.286$ s (g is the gravitational acceleration). Eight CCD cameras are arranged in parallel at the side of the flume to record the evolution of flow. These CCD cameras have a wide-angle lens for shooting 48 frames per second with a resolution of 1920×1440 (Liu et al., 2019a; Wang et al.,

2019). The cameras are simultaneously turned on by wireless remote control.

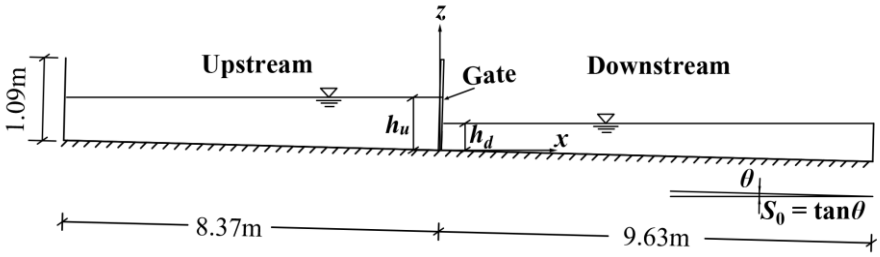

Fig. 1. Sketch of the flume device.

2.2. Image processing technology

The collection of experimental data by image processing technology involves two key parts. The first part is to use the calibration plate and the calibration function in MATLAB to individually calibrate each camera. The parameter data obtained (mainly the internal and external parameters of each camera) are then used to regulate the distorted picture. The size of the square lattice is 100 mm×100 mm in the calibration plate, and the number of the grid is 11 on one side, and 10 on the other side. Fifty-millimeter margin is set around the calibration plate to facilitate the recognition of the corner points. In order to obtain more accurate internal and external data for each camera, 25 pictures are used to calibrate each camera in different orientations and angles. The second part is to perform image analysis on the corrected image to obtain water depth data. The main purpose is to use the scale above the flume to cut and combine the images, and then to apply boundary recognition function to process the binarized image to obtain the variation of the water depth at each position. The actual length represented by a pixel is about 1.8 mm in the experiment (Liu et al., 2018, 2019b, Wang et al., 2019, 2020c).

This study is to examine the combined effect of the tailwater and bed slope on the propagation of dam-break flow. To this end, eleven downstream tailwater depths are tested for three different bed slopes. The parameters tested are listed in Table 1 in which $\alpha = h_d/h_u$ is the water depth ratio.

Tab. 1. Experimental parameters.

No.	h_u (m)	h_d (m)	α	S_0	No.	h_u (m)	h_d (m)	α	S_0
1	0.2	0	0	0	34	0.4	0	0	0
2		0.01	0.05	0	35		0.02	0.05	0
3		0.02	0.1	0	36		0.04	0.1	0
4		0.04	0.2	0	37		0.08	0.2	0
5		0.06	0.3	0	38		0.12	0.3	0
6		0.08	0.4	0	39		0.16	0.4	0
7		0.10	0.5	0	40		0.20	0.5	0
8		0.12	0.6	0	41		0.24	0.6	0
9		0.14	0.7	0	42		0.28	0.7	0
10		0.16	0.8	0	43		0.32	0.8	0
11		0.18	0.9	0	44		0.36	0.9	0
12	0.2	0	0	0.003	45	0.4	0	0	0.003
13		0.01	0.05	0.003	46		0.02	0.05	0.003
14		0.02	0.1	0.003	47		0.04	0.1	0.003
15		0.04	0.2	0.003	48		0.08	0.2	0.003
16		0.06	0.3	0.003	49		0.12	0.3	0.003
17		0.08	0.4	0.003	50		0.16	0.4	0.003
18		0.10	0.5	0.003	51		0.20	0.5	0.003
19		0.12	0.6	0.003	52		0.24	0.6	0.003
20		0.14	0.7	0.003	53		0.28	0.7	0.003
21		0.16	0.8	0.003	54		0.32	0.8	0.003

22		0.18	0.9	0.003	55		0.36	0.9	0.003
23	0.2	0	0	0.02	56	0.4	0	0	0.02
24		0.01	0.05	0.02	57		0.02	0.05	0.02
25		0.02	0.1	0.02	58		0.04	0.1	0.02
26		0.04	0.2	0.02	59		0.08	0.2	0.02
27		0.06	0.3	0.02	60		0.12	0.3	0.02
28		0.08	0.4	0.02	61		0.16	0.4	0.02
29		0.10	0.5	0.02	62		0.20	0.5	0.02
30		0.12	0.6	0.02	63		0.24	0.6	0.02
31		0.14	0.7	0.02	64		0.28	0.7	0.02
32		0.16	0.8	0.02	65		0.32	0.8	0.02
33		0.18	0.9	0.02	66		0.36	0.9	0.02

3. Results and discussion

3.1. Flow parameters

For the convenience, the following hydraulic parameters are defined to facilitate the analysis:

$$Z = \frac{z}{h_u} \tag{1}$$

$$T = \frac{t}{\sqrt{h_u / g}} \tag{2}$$

$$U = \frac{u}{\sqrt{g h_u}} \tag{3}$$

$$u_{(t)} = \frac{W_{(t+\Delta t)} - W_{(t)}}{bh\Delta t} \tag{4}$$

$$C = \frac{c}{\sqrt{gh_u}} \tag{5}$$

where z, t, and u respectively represent the water level, time, and mean velocity, Z, T and U are respectively the dimensionless water level, time and mean velocity, $u_{(t)}$ is the mean velocity at time t, The volume $W_{(t)}$ is calculated using the method similar to that by Cestero et al., (2014), Bento et al., (2017) and Melis et al., (2019), $W_{(t)}$ and $W_{(t+\Delta t)}$ is the water volume between a section and the upstream end of reservoir at the time t and $t+\Delta t$, respectively, Δt is the time step, taking as 1/48 s, b is the flume width, h is the water depth, c is the average wave celerity, calculated as $c = x_s/t$, x_s is the distance traveled by the wave over time t.

3.2. Observation of flow evolution pattern

Figs. 2 and 3 show the dam-break flow evolution for various tailwater and bed conditions for flat (Fig. 2(a), 3(a)), mild (Fig. 2(b), 3(b)) and steep bed slopes (Fig. 2(c), 3(c)). Fig. 2 is the flow pattern at the time t = 0.42 s with various water depth ratio. For the downstream dry bed (α = 0) because the gravity component in the flow direction does not exist for S_0 = 0 and is very small for S_0 = 0.003, the flow is mainly affected by the resistance in the wave-front. Therefore, the water depth becomes higher in the wave-front. For the case of steep slope S_0 = 0.02, the gravity component along the flow direction significantly increases, which accelerates the flow after being vector synthesized with the wave-front resistance. This makes water become thinner in the wave-front zone. For the case of downstream wet bed for all three bed slopes tested, the flow released from the reservoir interacts with downstream tailwater, producing an upwarp of water surface in the downstream. The height of such water upwarping decreases with the increase of α, as shown in Fig. 2.

Fig. 3 shows the flow pattern at t = 3.54 s in which different flow features occur after a period

of evolution. It is seen that for the case of dry bed, the wave-front spreads further and the water depth becomes smaller with the increase of bed slope. Both the rarefaction wave zone and steady zone are formed (Liu et al., 2019a; Wang et al., 2019) when α = 0.05−0.2, and the water level is almost horizontal in the steady zone for three different bed slopes. The instantly opening of the gate leads to a sudden flow discharge change in the channel. When the Froude number is less than 1.7, Favre waves will be formed in the channel (Treske, 1994). The reservoir area also appears this periodic wave phenomenon at S_0 = 0 and 0.003 for α = 0.3 by the instant opening of the gate. In order to distinguish it from the Favre wave which is formed downstream of the dam, these periodic waves appearing in the reservoir area are called extra negative waves (Kocaman and Ozmen-Cagatay, 2015; Liu et al., 2019a; Wang et al., 2019). In the case of steep bed slope (e.g. S_0 = 0.02), it is difficult for the extra negative waves to propagate upstream when α = 0.3, and there is no water surface fluctuation in the reservoir.

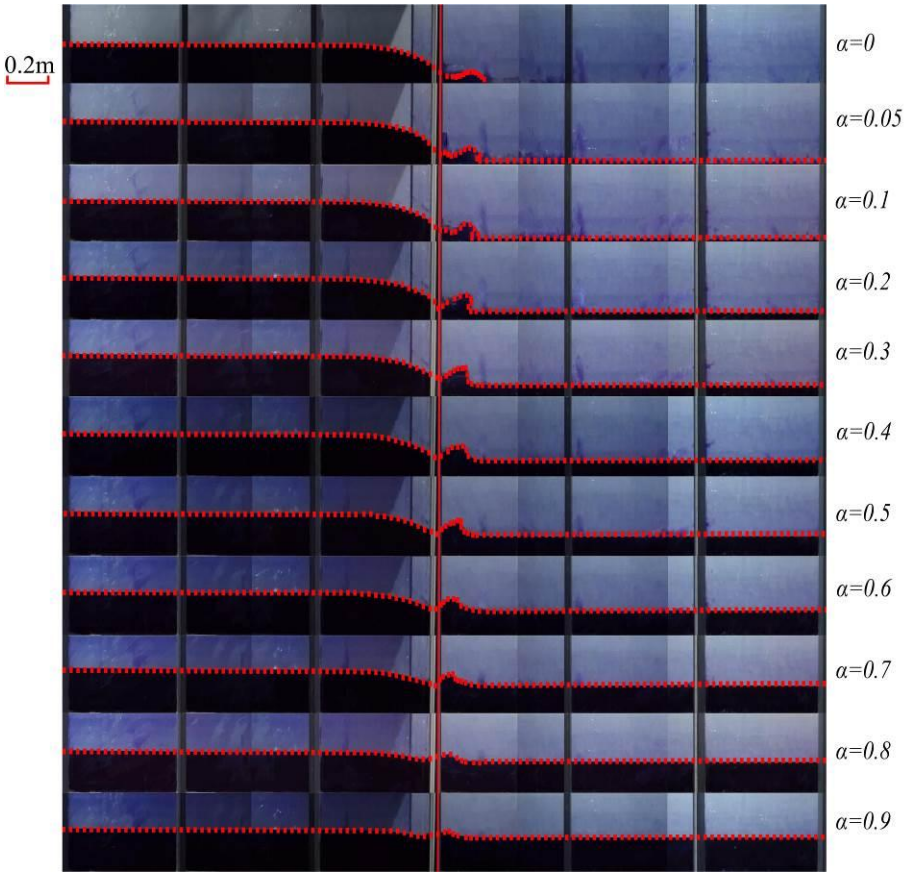
0.2m
α=0
α=0.05
α=0.1
α=0.2
α=0.3
α=0.4
α=0.5
α=0.6
α=0.7
α=0.8
α=0.9

186

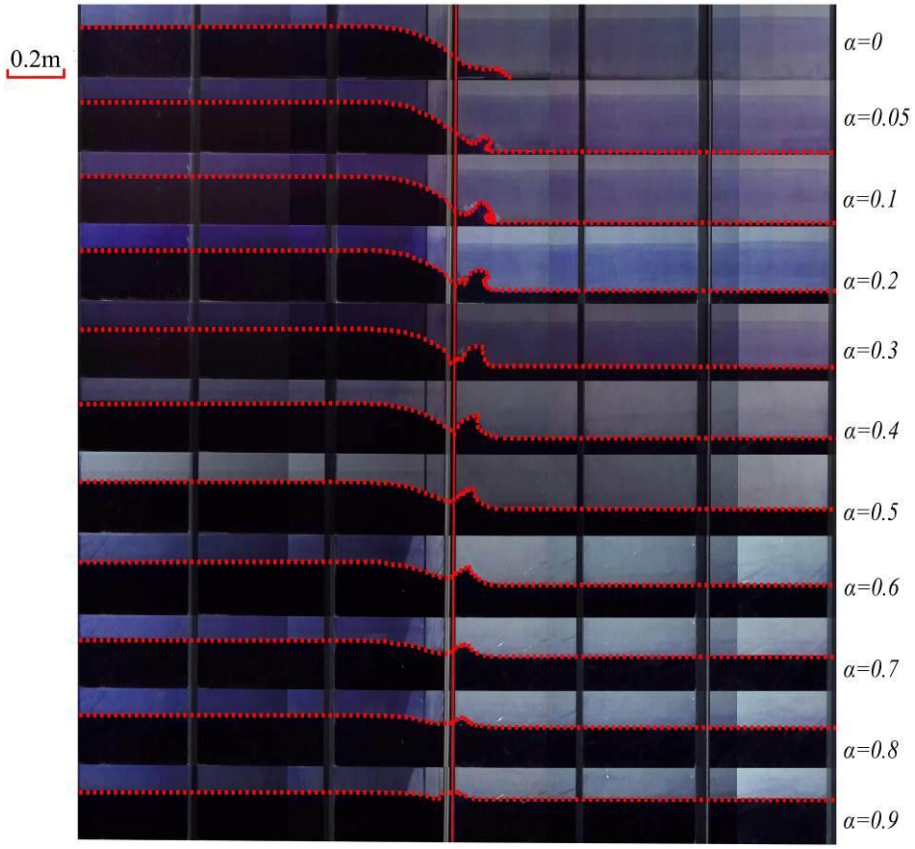
0.2m
α=0
α=0.05
α=0.1
α=0.2
α=0.3
α=0.4
α=0.5
α=0.6
α=0.7
α=0.8
α=0.9

187

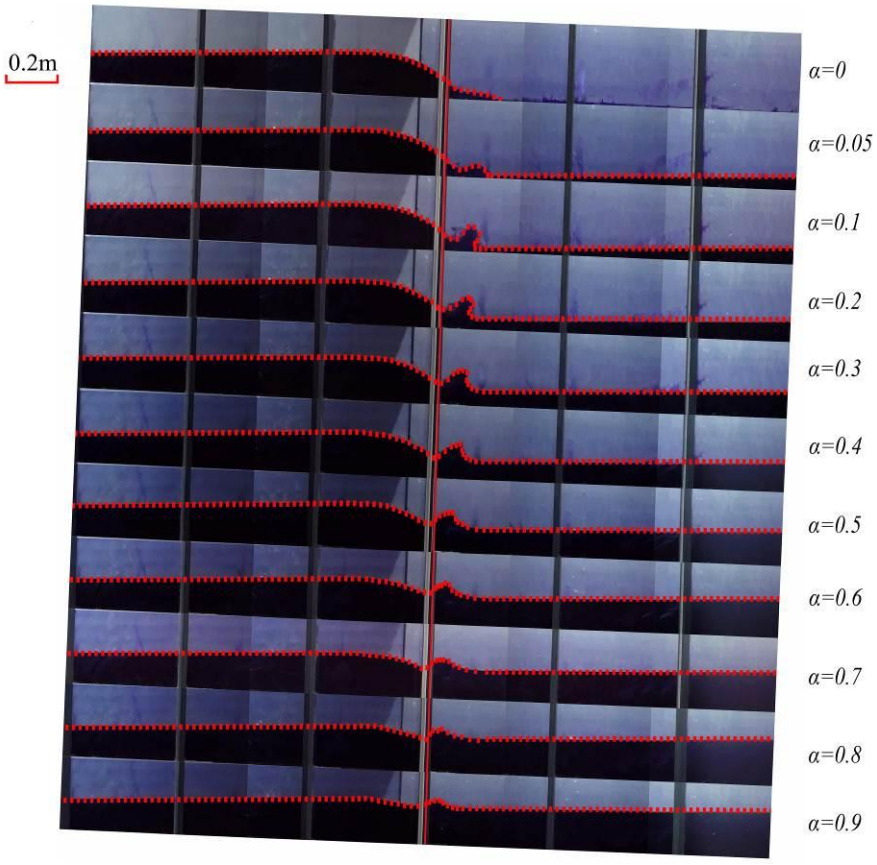

Fig. 2. Evolution pattern of the dam-break flows at t = 0.42 s (a) S_0 = 0; (b) S_0 = 0.003; (c) S_0 = 0.02.

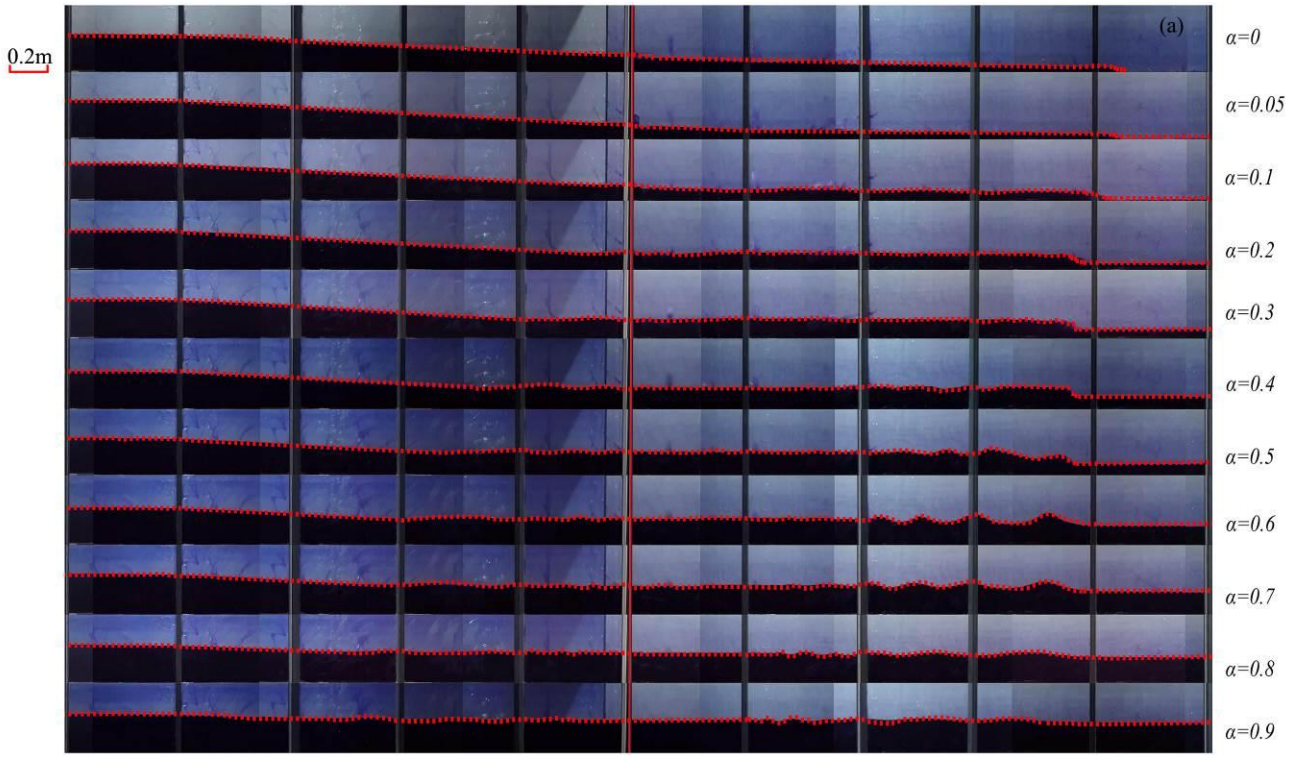

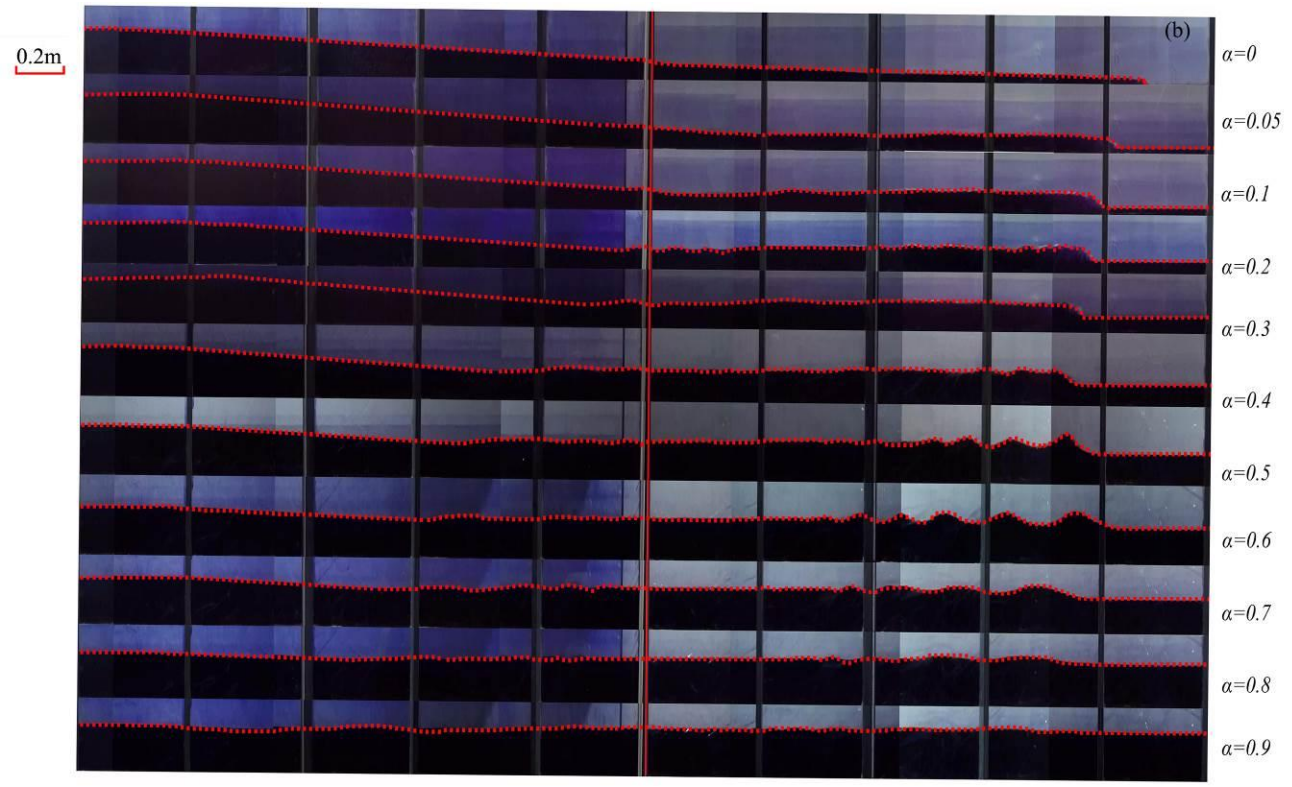

191

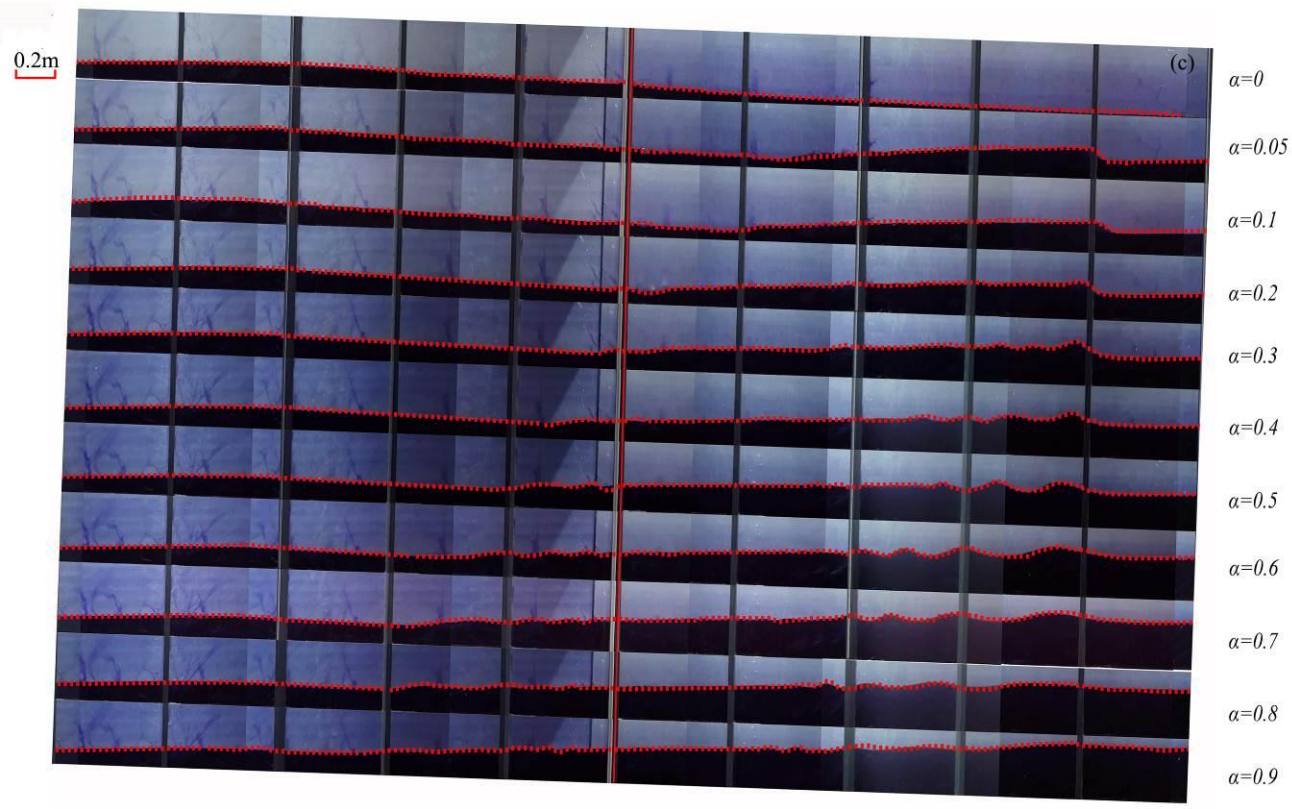

192

193 Fig. 3. Evolution pattern of the dam-break flows at t = 3.54 s (a) S_0 = 0; (b) S_0 = 0.003; (c) S_0 = 0.02.

194 Fig. 4 shows the evolution pattern of the Favre waves, in which the water surface undulates in the

195 wave-front when $\alpha \geq 0.4$. The first downstream wave (Soares-Frazao and Zech, 2002) is observed to

have a broken waveform when α = 0.4, 0.5, but a stable form when $\alpha \geq 0.6$. The difference between the bed slope S_0 = 0 and 0.003 with S_0 = 0.02 is that the water surface fluctuates in the wave-front when $\alpha \geq 0.3$, and the first downstream wave is broken at α = 0.3, 0.4 (the wave breaking condition is much weaker for α = 0.4 than α = 0.3)， and in a stable form when $\alpha \geq 0.5$. It shows that not only the depth of tailwater affects the propagation pattern of Favre waves, but also the bed slope plays a role.

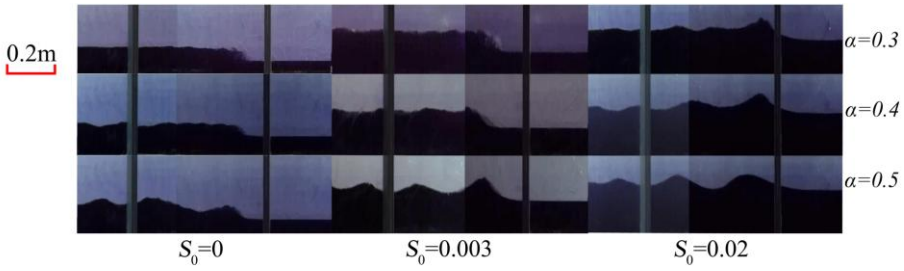

Fig. 4. Characteristics of the Favre waves under different bed slopes.

A generalized model is established to describe the evolution process of the dam break flow. Fig. 5 is a sketch of the flow pattern and parameters used to describe the flow development, in which c_n and c_w respectively represent the negative wave and the wave-front celerity, c_{en} and c_{es} respectively represent the celerities of the first extra negative wave and the first downstream wave, z_e represent the peak water level of the first extra negative wave, z_{max}, z_m, z_{min} respectively represent the maximum, average and minimum water level of the Favre waves, h_2 is the average water depth in the region of the Favre waves, h_0 is the downstream water depth connected with the first downstream wave front.

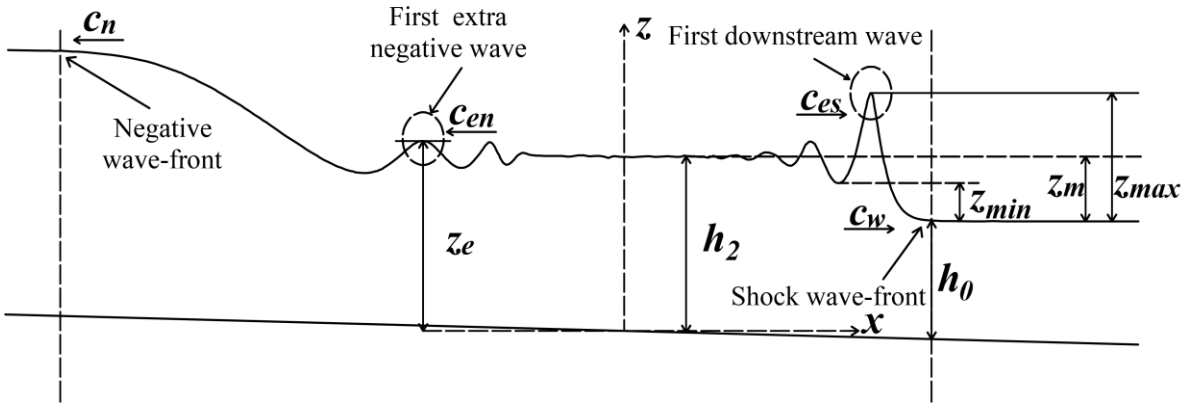

Fig. 5. Generalized model when waves appear upstream and downstream.

3.3. Water level

The variation of the water level for $\alpha = 0$ is shown in Fig. 6, where the measured data for $S_0 = 0$ have been published in Wang et al. (2020d). There is little difference of the water level for $h_u = 0.2$ m and $h_u = 0.4$ m for all bed slope conditions, indicating that the movement of dam-break flows meets the gravity similarity criterion. The analytical solutions of Chanson (2009) and Mungkasi and Roberts (2011) are also plotted in Fig. 6 for comparison. It is seen that the analytical solutions of Chanson (2009) and Mungkasi and Roberts (2011) of the water surface profiles are in good agreement with the measurements for the ideal zone where the effect of resistance is ignored for $S_0 = 0$. The main difference between them is that the wave-front zone is clearly affected by the resistance. The analytical solution of Chanson (2009) which considered the effect of wave-front resistance ($k_s = 10^{-5}$ m in this experiment) is in good agreement with the experimental results when $S_0 = 0$ and 0.003. The wave front velocity predicted by Mungkasi and Roberts (2011) who assumed that the channel was smooth (i.e. no wave-front resistance) is significantly larger than experimental measurement. As both the analytical solutions of Chanson (2009) and Mungkasi and Roberts (2011) didn't consider the characteristic of the initial water depth in the reservoir decreasing gradually along the direction towards the end of the reservoir, their predictions differ from the experimental results when $S_0 = 0.02$. In fact, the dimensionless water depth of the negative wave front position continuously decreases from 1 after the dam break begins, while it is always assumed to be 1 in the analytical. Nevertheless, the analytical solution of Chanson (2009) still has certain accuracy in capturing the position of the downstream wave-front when $S_0 = 0.02$.

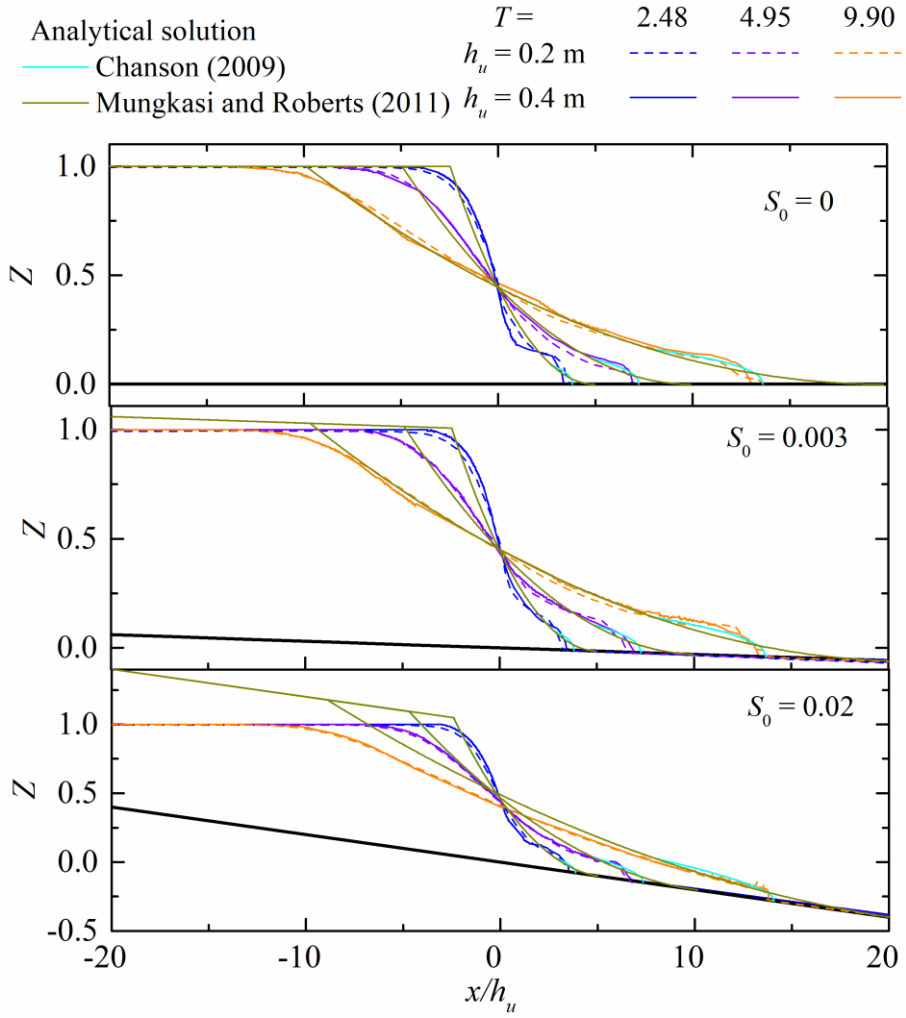

Fig. 6. Dimensionless free surface profiles for $\alpha = 0$.

When tailwater is present (e.g. downstream wet bed), the flow restores to stable state after the water upwarping at the initial time ($T = 2.48$) for $\alpha = 0.1$, as shown in Fig. 7, the rarefaction wave zone and steady zone can be seen at $T = 9.90$. It is worth noting that the dimensionless water level of the steady zone is almost the same under the three different bed slopes. The analytical solution of Mungkasi and Roberts (2012) is in good agreement with the experimental result at the wave-front position for T = 2.48 − 9.90 under the three different bed slopes. The water level in the steady zone calculated by Mungkasi and Roberts (2012) agrees well with the experimental result when the bed slope is small (e.g. $S_0 = 0.003$). However, large deviation between experiment and prediction of Mungkasi and Roberts (2012) exists for large bed slope, i.e. $S_0 = 0.02$. This may be ascribed to the

fact that the analytical solution of Mungkasi and Roberts (2012) was obtained based on the assumption that the water surface of the upstream and downstream still water zones was parallel to the channel bed, which was different from the horizontal water surface in the experiment.

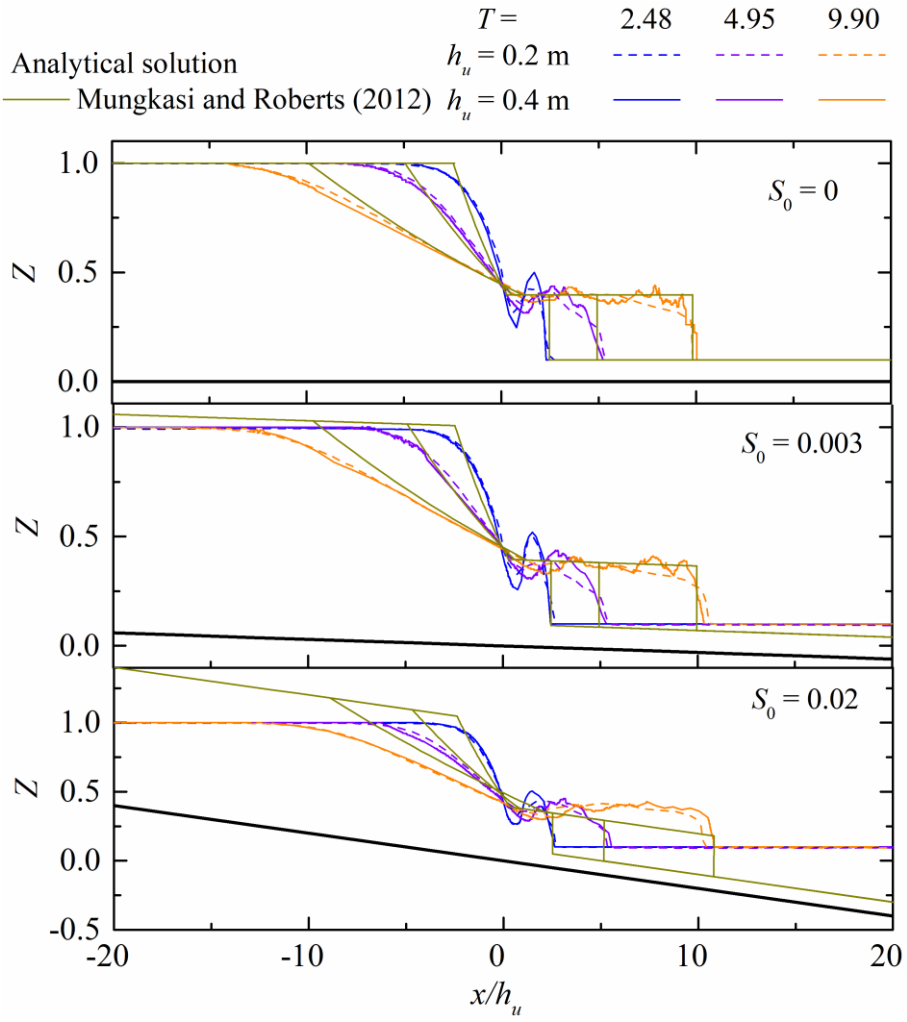

Fig. 7. Dimensionless free surface profiles for α = 0.1.

Fig. 8 shows that the second water upwarping occurs at T = 4.95 for α = 0.3. The analytical solution of Mungkasi and Roberts (2012) is plotted in Fig. 8 for comparison. It is seen from Fig. 8 that the dimensionless water level also has little difference in the steady zone for three different bed slopes. When α = 0.5, because the first downstream wave is broken during the evolution process for S_0 = 0 and 0.003, the water level is lower than S_0 = 0.02 (the first wave propagates in a stable form in this α). The periodic waves appear both in the reservoir area and downstream of the dam when α

increases to 0.7. The water level in the steady zone calculated by Mungkasi and Roberts (2012) is in good agreement with the measurements for α = 0.3 when S_0 = 0 and 0.003. However, when the water depth ratio increases to 0.5, 0.7, the analytical solution of Mungkasi and Roberts (2012) cannot capture the water surface fluctuations regardless of the bed slope. This is because the analytical solution of Mungkasi and Roberts (2012) was derived based on the shallow water assumption which is not suitable to describe the weak non-hydrostatic flow phenomenon (e.g. Favre waves). Such flow phenomenon is better described by the theory proposed by Soares-Frazao and Zech (2002).

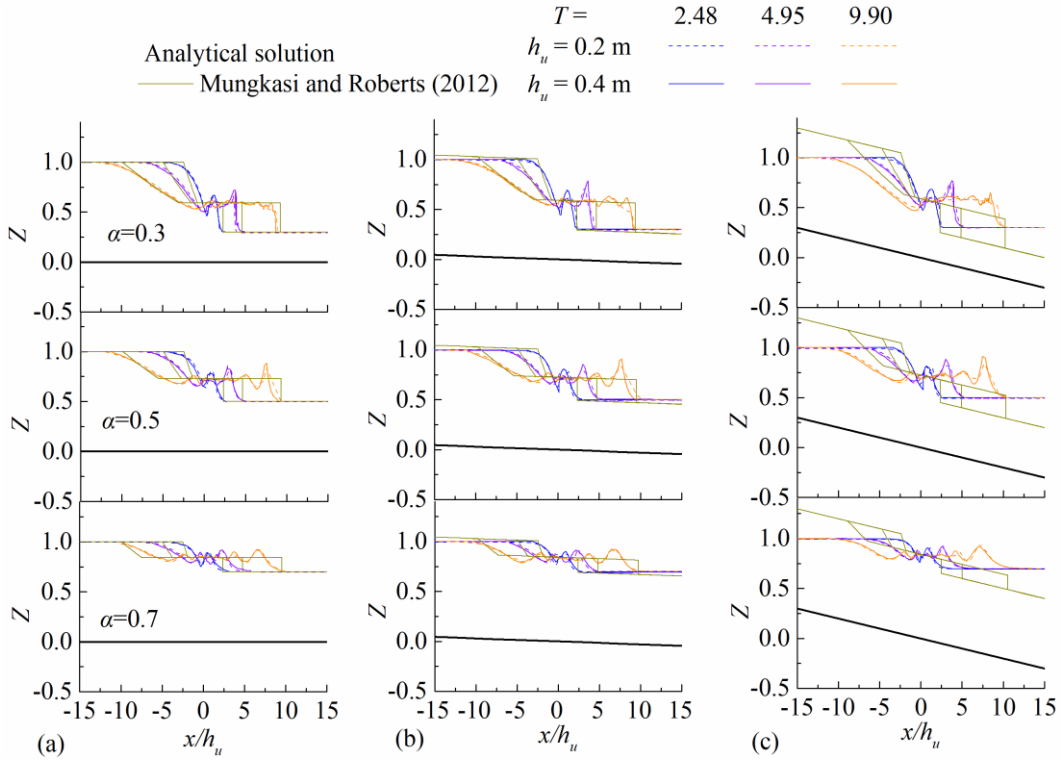

Fig. 8. Dimensionless free surface profiles for (a) α = 0.3; (b) α = 0.5; (c) α = 0.7.

Fig. 9 shows the stage hydrographs at the positions x/h_u = −12.8, −1.3, 0.8, 12.5 for downstream dry bed. The stage hydrographs are almost the same in the reservoir area for S_0 = 0 and 0.003, but it is gradually separated from S_0 = 0 and 0.003 after T = 5 at position x/h_u = −1.3 for S_0 = 0.02, in which the water level decreases. At the position x/h_u = −12.8, water level for steep slope S_0 = 0.02 begins to fall later than that for flat and mild slopes (e.g. S_0 = 0 and 0.003). The decline velocity

271 of water level is further accelerated at T = 28 when S_0 = 0 and 0.003 with h_u = 0.4 m. This may be
272 ascribed to the fact that the celerity of negative wave is faster when h_u = 0.4 m than that with h_u = 0.2
273 m, and the decline of the water level at the end of the reservoir will further affect the variation
274 process of the water level in the reservoir area. Therefore, the phenomenon of stage hydrograph
275 separation occurs at this time. This phenomenon appears at T = 32 for S_0 = 0.02, which shows that
276 the increase of the bed slope not only delays the evolution of the negative wave, but also delays the
277 time when the water level is further declined in the reservoir area. The water level variation in the
278 reservoir area predicted by Chanson (2009) is the same as that predicted by Mungkasi and Roberts
279 (2011). In the case of S_0 = 0 and 0.003, they both can relatively accurately predict the variation of the
280 water level in the reservoir area. However, in the case of S_0 = 0.02, the predicted water level at the
281 position x/h_u = −1.3 continues to rise in the later period (i.e. T > 12), which is different from the
282 experimental results. For the comparison of the water level downstream of the dam, the analytical
283 solution of Chanson (2009) accurately captures the rising time of the water level at the downstream
284 location as it considered the effect of wave-front resistance. The predicted variation of the water
285 level is in good agreement with the experimental result when S_0 = 0 and 0.003, while the prediction
286 deviates significantly from the experimental results when S_0 = 0.02.

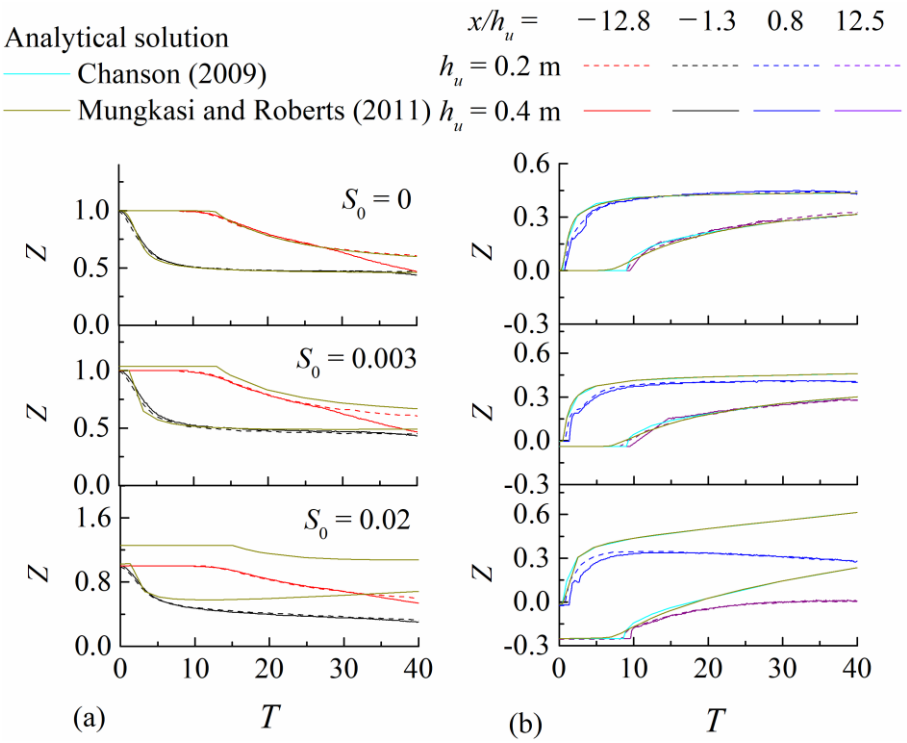

Fig. 9. Stage hydrographs for α = 0 (a) reservoir area; (b) downstream of the dam.

Figure 10 shows the variation of the water level in both the reservoir area and downstream of the dam for α = 0.1. The characteristics of the water level variation in the reservoir area is very similar to that for α = 0. The water level at the downstream of the dam gradually becomes stable after a short time rising. The analytical model of Mungkasi and Roberts (2012) can accurately predict the variation of the water level for S_0 = 0 and 0.003. However, for S_0 = 0.02, the water level at x/h_u = 0.8 predicted by Mungkasi and Roberts (2012) differs from the experimental measurement. This deviation may be ascribed to the fact that the location x/h_u = 0.8 gradually evolves from the steady zone to the rarefaction wave zone and the water level then continues to rise. The situation at the position x/h_u = 12.5 is similar with a longer transition time from the steady zone to rarefaction wave zone.

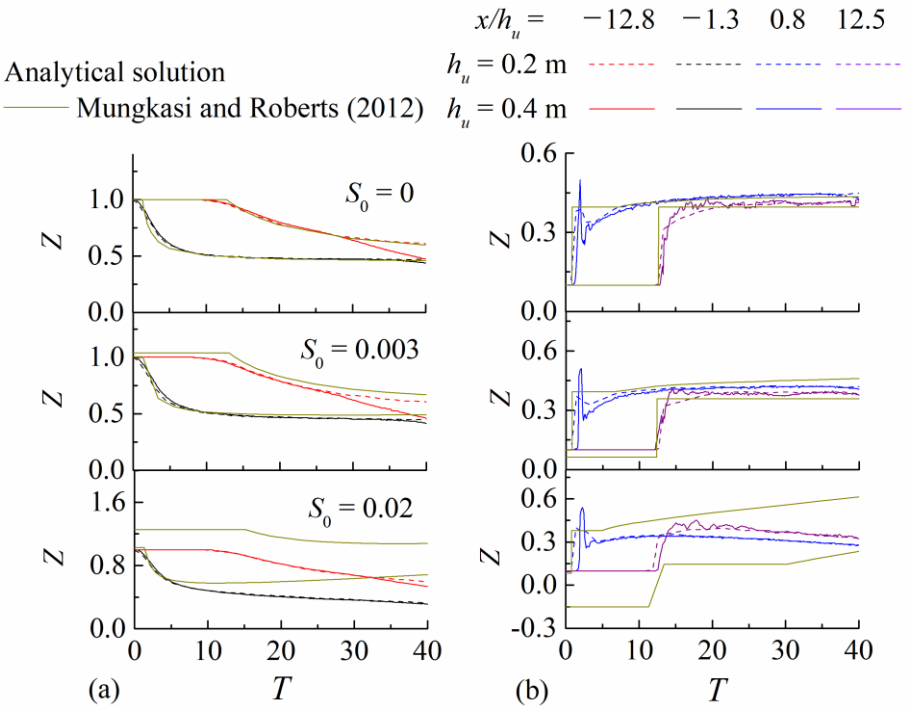

Fig. 10. Stage hydrographs for α = 0.1 (a) reservoir area; (b) downstream of the dam.

Fig.11 shows the water level at each position for $\alpha \geq 0.3$. The water level at $x/h_u = -1.3$ fluctuates significantly for S_0 = 0 and 0.003 and α = 0.3. Such water level fluctuation is very small for S_0 = 0.02, which is consistent with the characteristics observed in Section 3.2 in which the extra negative waves are difficult to propagate towards the reservoir area. When the water depth ratio further increases (e.g. α = 0.5), periodic water level fluctuations occur both in the reservoir area and downstream of the dam. When the water depth ratio further increases to α = 0.7, the frequency of fluctuations increases, while the flow has the characteristics of Favre waves (Soares-Frazao and Zech, 2002). Fig. 11 shows that the analytical solution of Mungkasi and Roberts (2012) which was obtained based on the shallow water assumption is unable to capture the wave characteristics.

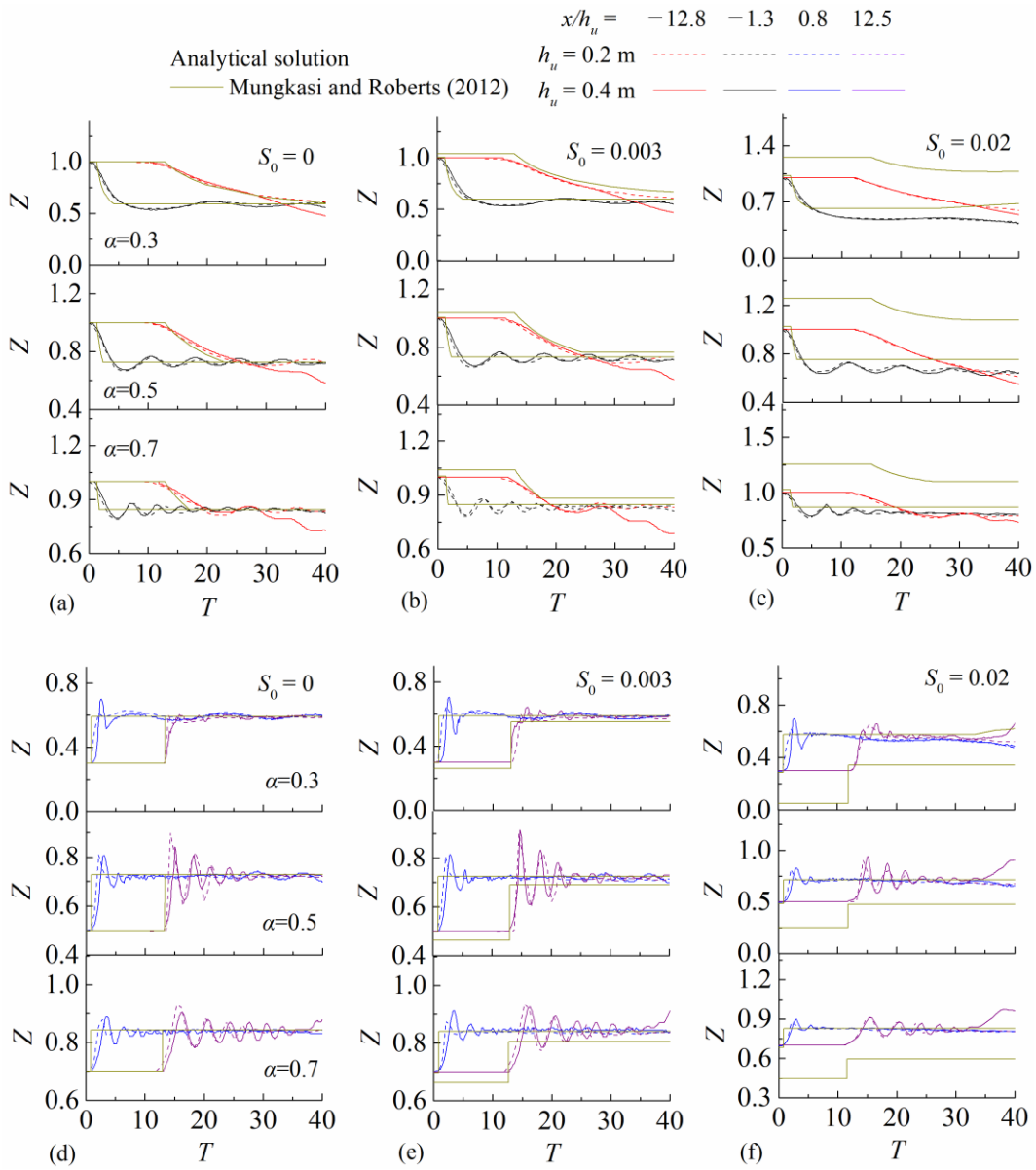

Fig. 11. Stage hydrographs for α = 0.3, 0.5, 0.7 (a) − (c) reservoir area; (d) − (f) downstream of the dam.

3.4. Mean velocity

Fig. 12 shows the dimensionless mean velocity profiles, where the measured data for S_0 = 0 have been published in Wang et al. (2020d). The flow velocity increases continuously with time, and the peak velocity appears in the wave-front for downstream dry bed. When there is downstream tailwater, the situation is different. It is seen that for α = 0.1 and flat/mild bed slope (e.g., S_0 = 0 and 0.003),

flow velocity approaches a steady value in the steady state region, while for steep slope (e.g., S_0 = 0.02), the flow velocity gradually decreases after reaching the peak. When tailwater depth downstream increases to α = 0.3, the position of the maximum flow velocity moves towards the reservoir area. For a higher α (e.g., 0.5 and 0.7), there is a wave variation for the velocity distribution in both upstream and downstream reaches.

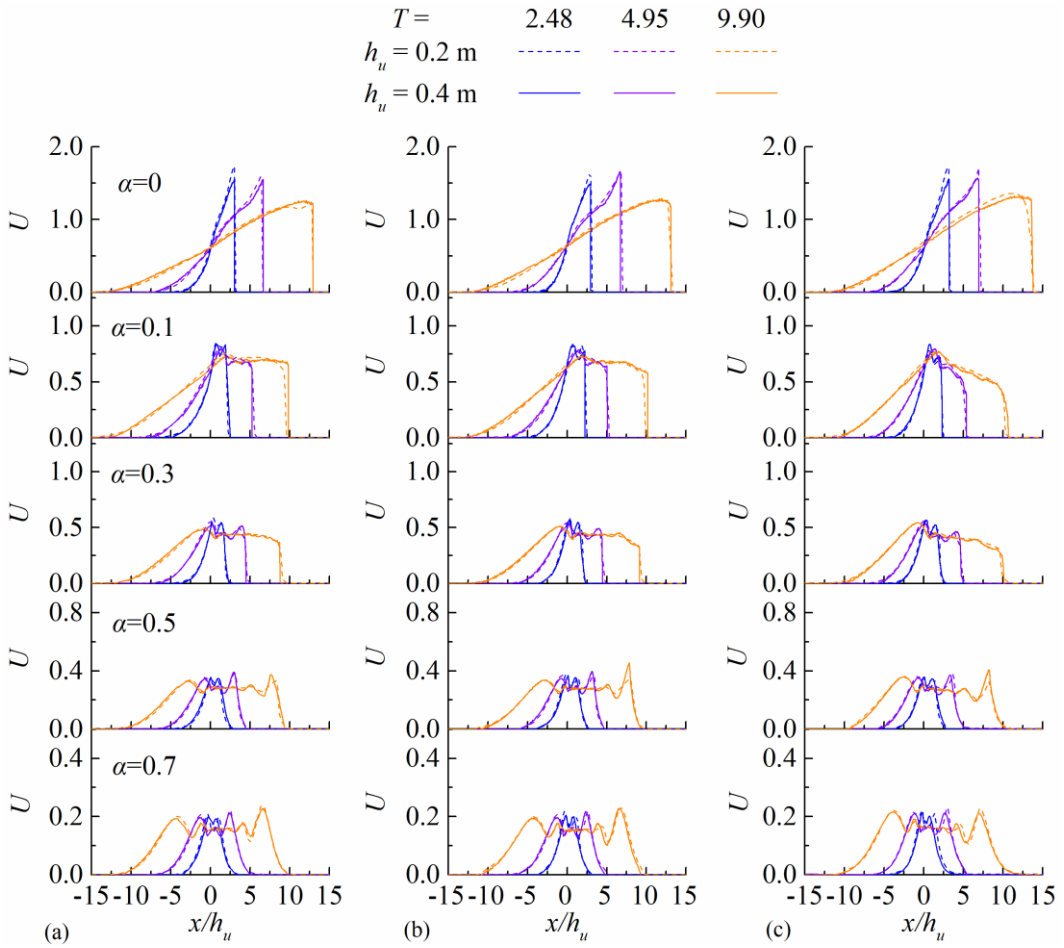

Fig. 12 Dimensionless mean velocity profiles (a) S_0 = 0; (b) S_0 = 0.003; (c) S_0 = 0.02.

Fig. 13 shows that the flow velocity at x/h_u = −1.3 gradually decreases in the later stage for S_0 = 0 and 0.003 with downstream dry bed, while for S_0 = 0.02, flow velocity still gradually increases. For h_u = 0.4 m, the flow velocity gradually decreases in the later stage at position x/h_u = −12.8. Since the celerity of negative wave is slower when h_u = 0.2 m, the significant decline of the flow velocity appears later correspondingly. The change characteristics for α = 0.1 is similar to that of downstream

dry bed. For high downstream water depth (e.g. $\alpha > 0.3$), flow velocity fluctuates at $x/h_u = -1.3$, which is affected by the extra negative waves. Such fluctuation frequency gradually increases as α increases. From the variation of flow velocity at position $x/h_u = -12.8$, it can be seen that the impact of such fluctuation spreads faster to the reservoir area for $\alpha = 0.7$ than that for $\alpha = 0.5$.

For the position downstream of the dam, the flow velocity has a steep rise and then slowly declines in dry bed condition. The flow velocity gradually recovers to a stable value after a sharp rise when $\alpha = 0.1, 0.3$, but from the change of the flow velocity at position $x/h_u = 12.5$, it can be seen that the stable value for $S_0 = 0.02$ is smaller than that for $S_0 = 0$ and 0.003. This could be explained as follows: in the case of a downstream wet bed, the water depth is relatively larger at position $x/h_u = 12.5$ for $S_0 = 0.02$. The flow velocity gradually becomes stable after the fluctuation at $x/h_u = 0.8$ when $\alpha = 0.5$ and 0.7. Since the water depth at $x/h_u = 12.5$ is larger for $S_0 = 0.02$, the energy is dissipated faster, and thus, the flow velocity begins to decrease earlier compared to that for $S_0 = 0$ and 0.003.

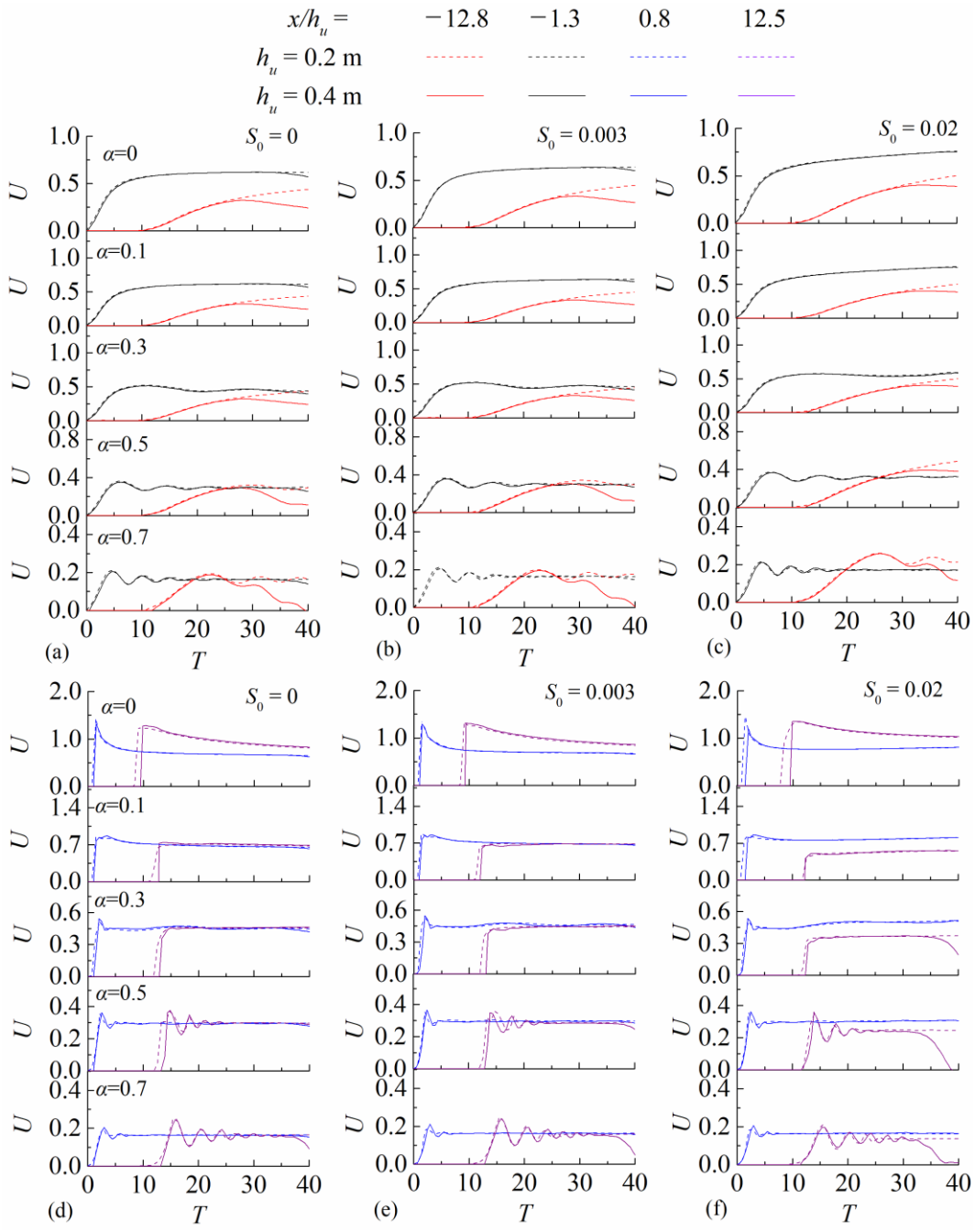

344

345 Fig. 13 Dimensionless mean velocity distribution at different locations (a) − (c) reservoir area; (d) −

346 (f) downstream of the dam.

347

3.5. *Wave celerity*

3.5.1. Negative wave and wave-front

Fig. 14 shows the variation of the average negative wave celerity with time. It is seen that the negative wave celerity sharply decreases with time at the initial stage ($T < 5$) and then gradually decreases and approaches a steady state for $S_0 = 0$. Due to the effect of the bed slope, there is an added horizontal acceleration on the flow, which is opposite to the negative wave propagation direction. Therefore, the negative wave celerity will gradually decrease at the later stage under the situation of the bed slope $S_0 = 0.003$ and 0.02. The analytical solutions of Dressler (1958), Chanson (2009) and Mungkasi and Roberts (2011) have the same dimensionless negative wave celerity which is equal to 1 for a horizontal bed. However, for bed slope is larger than zero (i.e. $S_0 = 0.003$ and 0.02 in this study), the dimensionless negative wave celerity continuously decreases with time. The analytical solutions of Chanson (2009) solution and the Mungkasi and Roberts (2011) have exactly the same negative wave celerity for three different bed slope conditions. The negative wave celerity predicted by Dressler (1958) decreases slower than those predicted by Chanson (2009) and Mungkasi and Roberts (2011) and it has a tendency to be close to the experimental results with the evolution of the dam-break flow. The negative wave celerity predicted by Mungkasi and Roberts (2012) deviates relatively small from the experimental results for $S_0 = 0.003$ and $\alpha = 0.1$. With the increase of the water-depth ratio, the predicted negative wave celerity improves. For the steep bed slope $S_0 = 0.02$ with wet bed condition, there exists relatively large difference between the analytical calculation and experimental measurements for all water depth ration investigated here.

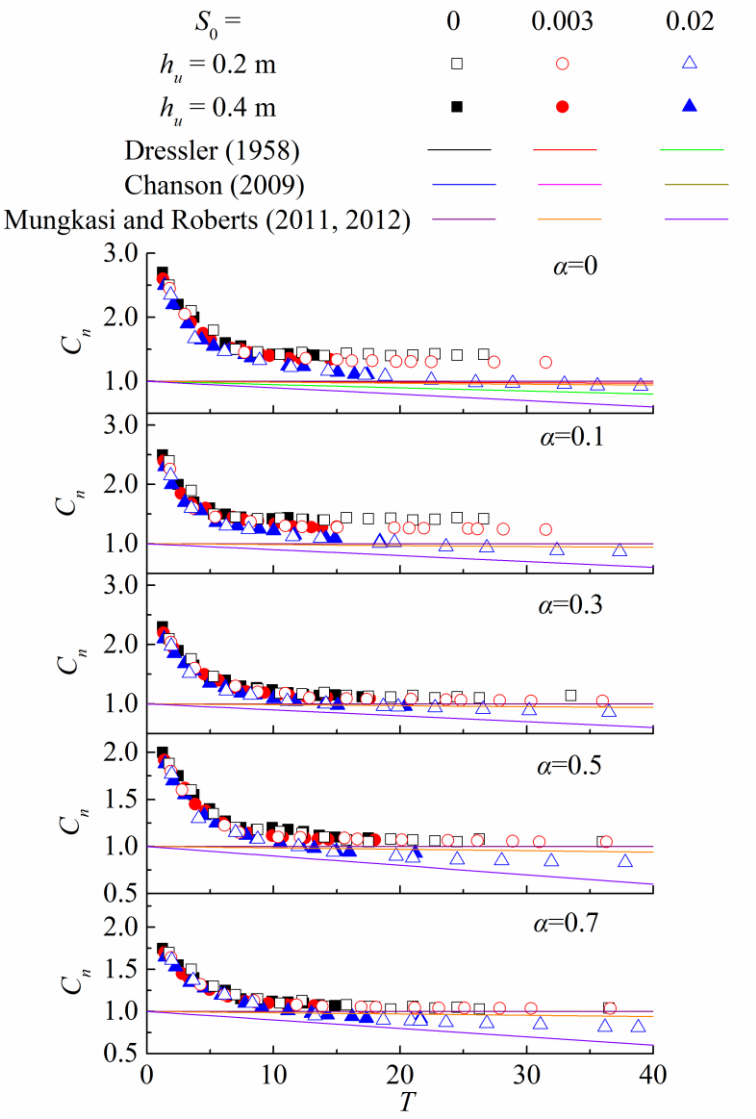

Fig. 14. Variation of dimensionless average negative wave celerity with time for various water depth ratio and bed slopes.

Fig. 15 shows the variation of the average wave-front celerity with time. It is seen that the bed slope has a great effect on the wave-front celerity. Owing to the still water in the downstream of the dam has greater resistance compared to the dry bed case, it is shown that the wave-front celerity in the dry bed case is significantly larger than that in wet bed case. Analytical solutions of Dressler (1958), Chanson (2009) and Mungkasi and Roberts (2011, 2012) are plotted in Fig. 15 for comparison. It shows that the wave-front celerity predicted by Dressler (1958) is similar to that predicted by Mungkasi and Roberts (2011) for three different bed slopes. As the influence of the

wave-front resistance is not considered in both analytical solutions, the wave-front celerity continuously increases with time for the bed slope S_0 = 0.003 and 0.02 and the dimensionless celerity is much larger than the experimental measurement. Chanson (2009) considered the wave-front resistance effect and the predicted wave front celerity is in good agreement with the measurements. The wave-front celerity of Mungkasi and Roberts (2012) does not change with time on the horizontal bed, and it is in good agreement with the experimental results. It is slowly increasing at S_0 = 0.003, and has little different with the experimental results. But in the case of S_0 = 0.02, the wave-front celerity rises faster, which is coordinate with the experimental situation in the early stage (almost T = 15), but in the later stage, the celerity is faster than the experimental situation. It is analyzed that there will be more energy dissipation in the interaction between the wave-front and the downstream still water in the experiment, and the acceleration will change instead of keeping a fixed value like the analytical solution.

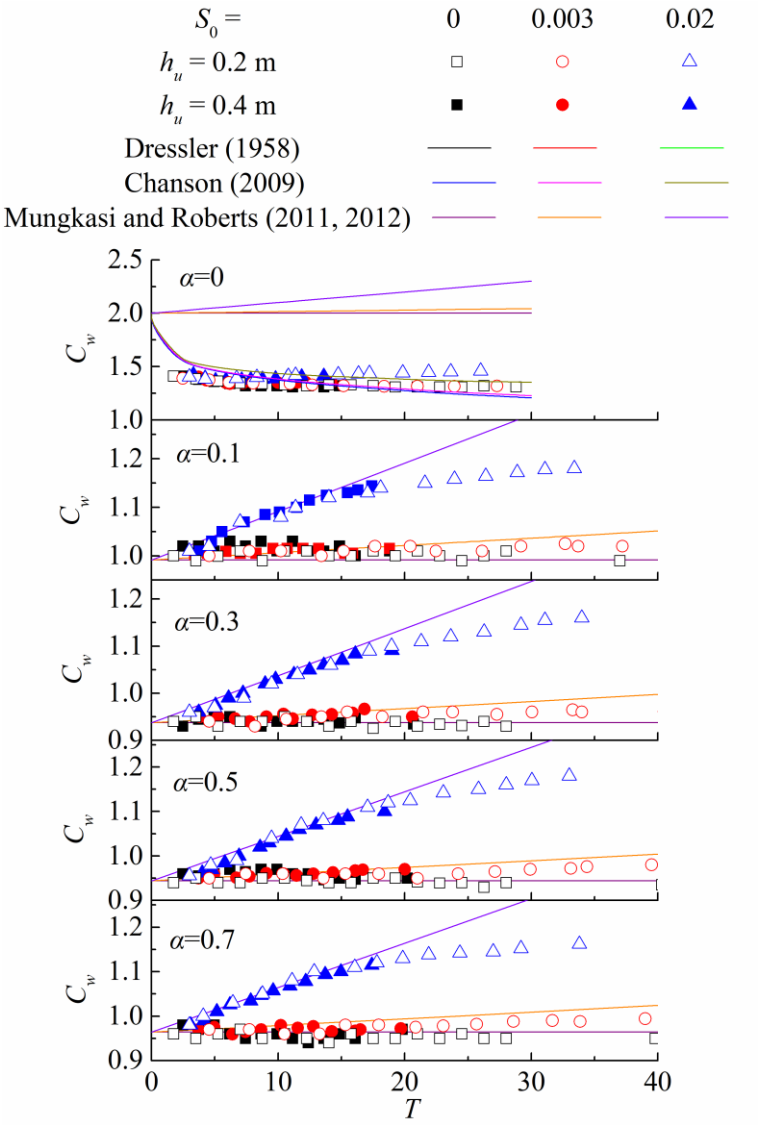

Fig. 15. Effect of the bed slope and water depth ratio on the dimensionless average wave-front celerity.

3.5.2. First extra negative wave and first downstream wave

Experimental results show that the periodic waves will not only propagate downstream, but also appear in the reservoir area. For rivers/channels with cascade regulation mechanism, such periodic waves will propagate towards upstream when the gate is used to adjust the discharge. This will have an adverse effect on upstream structures or the navigation of upstream vessels. Therefore it is also important to investigate the propagation of the extra negative waves. Figs. 16 and 17 are respectively

399 the variation of the dimensionless average celerity of the first extra negative wave and the first
400 downstream wave with time for various α and bed slopes. It is seen that the dimensionless celerity of
401 the first extra negative wave has great consistency between h_u = 0.2 m and h_u = 0.4 m, and the same
402 for the dimensionless celerity of the first downstream wave. The celerity of both the first extra
403 negative wave and the first wave increases with time, reaches a maximum and then decreases with
404 time. Fig. 16 also shows that the celerity of the first extra negative wave propagating along the steep
405 slope (S_0 = 0.02) is smaller than that along the flat and mild slope. Such difference increases with the
406 increase of the evolution time. While for the celerity of the first wave, the situation is another way
407 round. The celerity of the first wave is larger along the steep slope (S_0 = 0.02) than that along the flat
408 and mild slope (S_0 = 0 and 0.003) due to the promoting effect of gravity component in the horizontal
409 direction.

410 The following empirical formulas are developed for the first extra negative wave celerity (Eq.
411 (6)) and the first downstream wave celerity (Eq. (7)):

$$C_{en} = -1.75\times10^{-6}\times T^3 - 0.009\times S_0^{1.18}\times T^2 + 0.0135\times T + 0.67\times\alpha - 0.38 \quad (6)$$

$$C_{es} = -2.6\times10^{-6}\times T^3 + 0.003\times S_0\times T^2 + 0.009\times T - 0.26\times\alpha + 0.82 \quad (7)$$

412 the correlation coefficient R^2 is applied to analyze the fitting results. Fig. 18 shows the comparison of
413 experimental measurements and the fitted data calculated using Eqs. (6) and (7). The good agreement
414 between the calculated and measured data indicates that Eqs. (6) and (7) can be used to quickly
415 estimate the wave celerity and provide a certain reference for engineers in actual design and
416 operation.

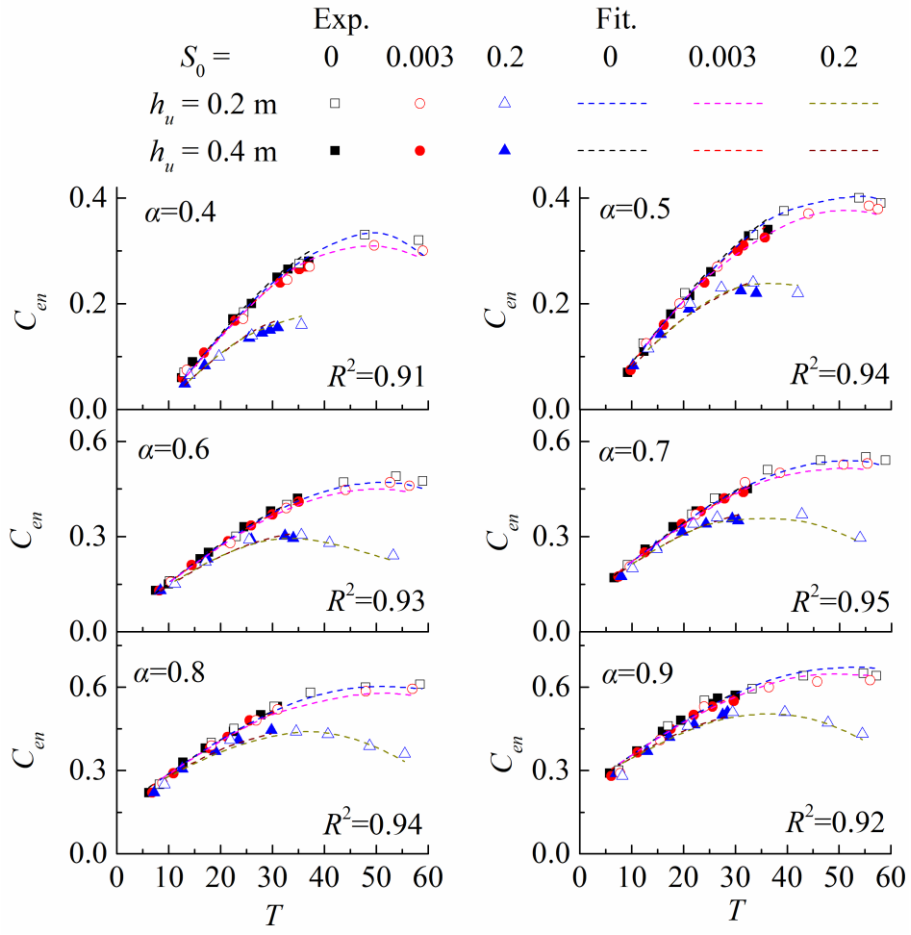

417

418 Fig. 16. Dimensionless average celerity of the first extra negative wave.

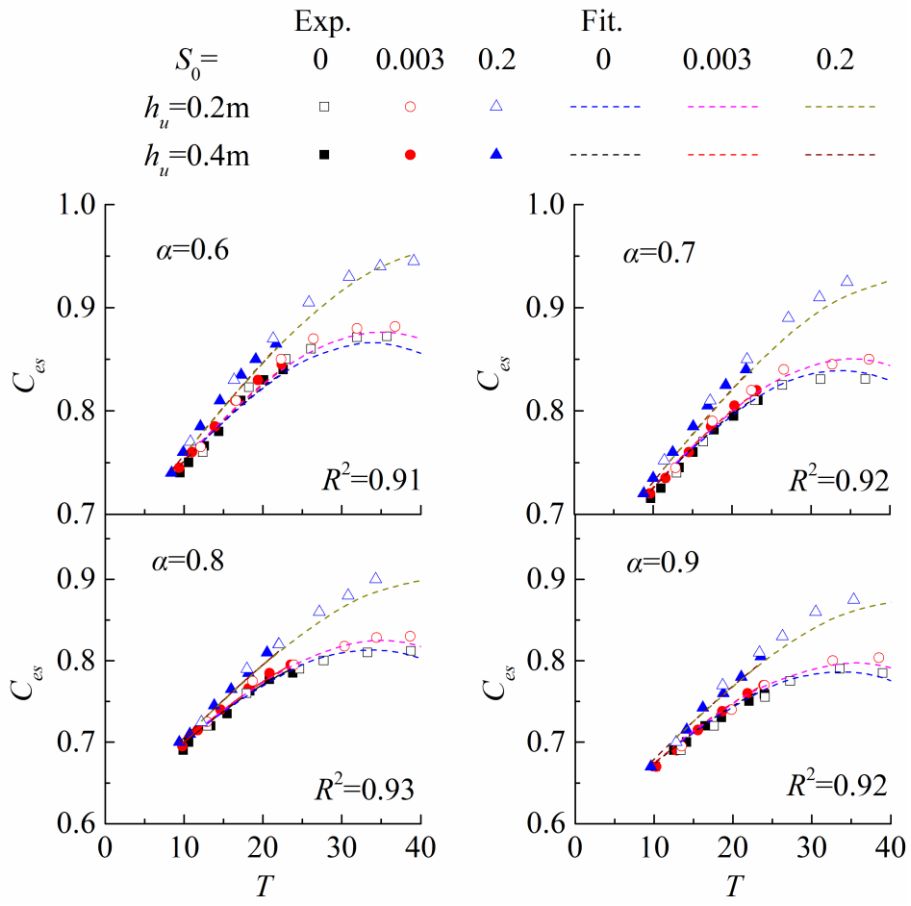

Fig. 17. Dimensionless average celerity of the first downstream wave.

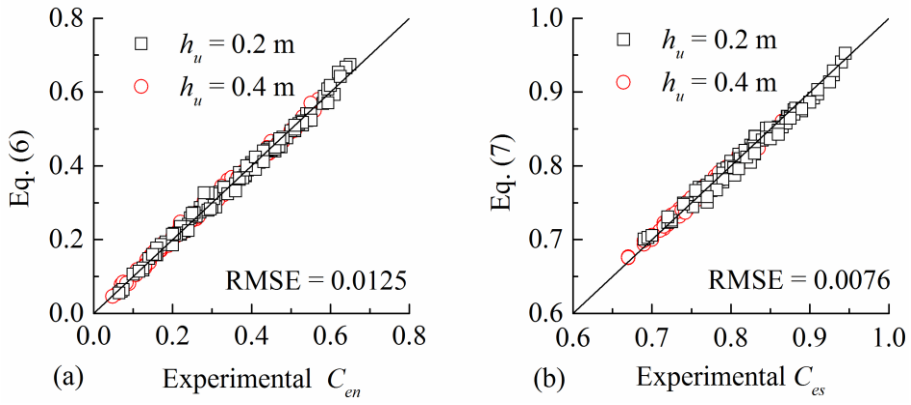

Fig. 18. Comparison of experimental measured and calculated results using Eqs. (6) and (7) for (a) C_{en}; (b) C_{es}

3.6. Wave height

427 **3.6.1. Favre waves**

428 *Fr* is a characteristic parameter for analyzing Favre waves and can be calculated as (Treske,
429 1994):

$$Fr = \frac{\omega}{C_0} = \frac{C_a - U_0}{C_0} \tag{8}$$

430 where ω is the relative propagation speed to the base flow U_0 which is 0 in the present study, C_a
431 is the absolute propagation speed of the first downstream wave front, C_0 is the wave speed
432 $C_0 = \sqrt{gh_0}$ (h_0 is water depth immediately in the front of the first downstream wave). Soares-Frazao
433 and Zech (2002) obtained the formula $Fr = \sqrt{\frac{h_2}{2h_0^2}(h_2 + h_0)}$ which is the application of Eq. (8) for the
434 case of horizontal bed. For convenience of comparison of the results with different bed slopes, the Eq.
435 (8) is used for calculation (Treske, 1994). Figure 19 shows the calculated *Fr* at water depth ratios α =
436 0.3 and α = 0.5. It can be seen that under horizontal bed condition, *Fr* has little variation with time
437 and is greater than 1.28 for both water depth ratios investigated (i.e. α = 0.3 and α = 0.5). The
438 wave-front shows a steep or broken form which is consistent with the description of Soares-Frazao
439 and Zech (2002). For bed slope S_0 =0.003, *Fr* decreases with time for α = 0.3, but it is also greater
440 than 1.28 and the wave-front is also steep, which is consistent with the observation in Figure 4. *Fr* is
441 very close to 1.28 at the late evolution for α = 0.5. However, *Fr* significantly decreases at S_0 =0.02.
442 This is because the water depth of the downstream still water which is interacted with the wave-front
443 continues to increase, indicating that more energy will be dissipated downstream. Fig. 19 (a) also
444 shows that *Fr* is very close to 1.28 (*Fr* = 1.297) at the late stage (i.e. *T* = 34) for S_0 = 0.02 and α = 0.3.
445 It is expected that if the flow continues to evolve (limited by the length of the flume available for
446 measurement downstream of the dam in this study, which limits the maximum evolution time being

447 approximately $T = 34$ for $h_u = 0.2$ m), it will also produce stable Favre waves.

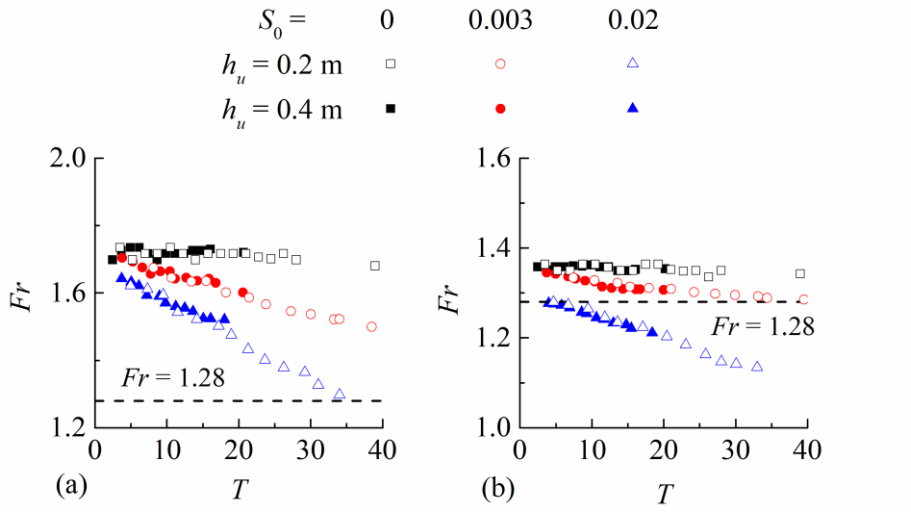

448

449 Fig. 19. Variation of *Fr* in different bed slopes for (a) $\alpha = 0.3$; (b) $\alpha = 0.5$.

450

451 Figure 20 shows the comparison of the measured parameters of Favre wave under the horizontal
452 bed with the previous results (Favre, 1935; Sandover and Zienkiewicz, 1957; Treske, 1994; Marche
453 et al., 1995; Soares-Frazao and Zech, 2002; Bishnu et al., 2009). It can be seen that z_{max} initially
454 increases with the increase of *Fr* and then decreases significantly after $Fr > 1.28$, due to the wave
455 breaking). The experimental result is in good agreement with that observed by Treske (1994). The
456 change of z_m increases almost linearly with *Fr*, which is also well predicted by Eq. (8). It is also seen
457 that z_{min} increases gradually with the increase of *Fr* and has a sharp increase when *Fr* is larger than
458 1.28.

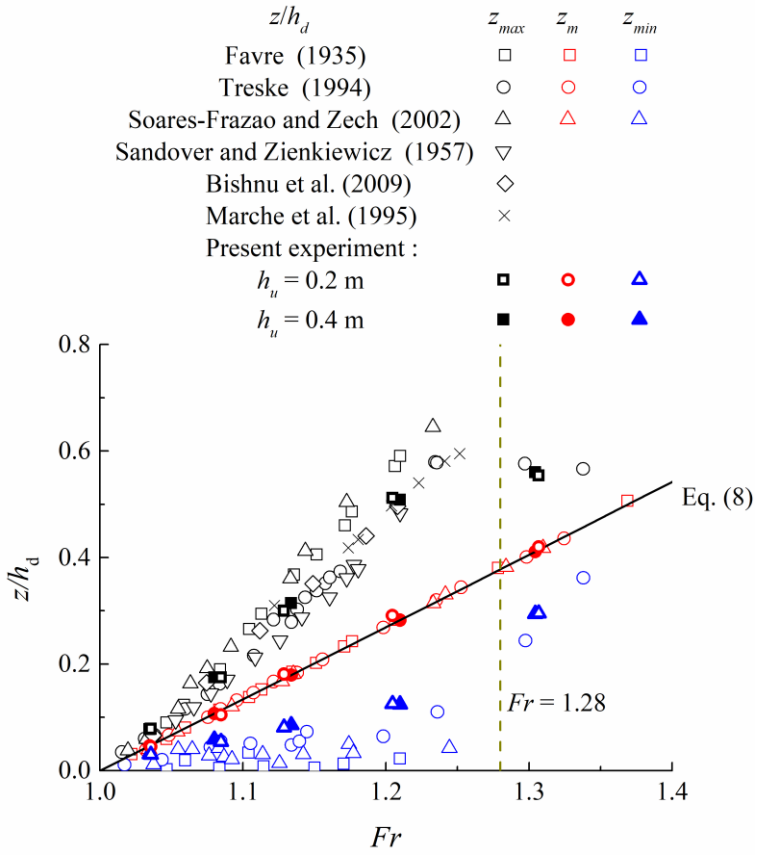

Fig. 20. Comparison of characteristics of Favre waves.

In addition，the maximum value of the wave-front height (z_{max}) determines the highest water level when the flood develops towards downstream. Fig. 21 shows the wave-front height for various test conditions (the wave-front height is calculated using the water level in the steady zone when $\alpha \leq 0.4$). It is seen that the variation of the wave-front height with α has a double-peak. The maximum value of the wave-front height appears at $\alpha = 0.2$, and the dimensionless height is approximately 0.31. The wave-front height reaches the second peak at $\alpha = 0.6$ and decreases sharply with the increase of α. It is shown that the bed slope and downstream water depth has an insignificant effect on the dimensionless wave-front height, particularly when $\alpha \geq 0.6$ which is influenced by Favre waves.The wave-front height predicted by Mungkasi and Roberts (2012) (solid line) is the same for three different bed slopes and is in good agreement with the experimental measurement for $0 < \alpha \leq 0.4$. However, the analytical model significantly under-predict the wave-front height when the Favre

wave occurs. This indicates that the shallow water assumption is not suitable for describing the phenomenon of weak non-hydrostatic flow when the water depth ratio is large, as evidenced previously.

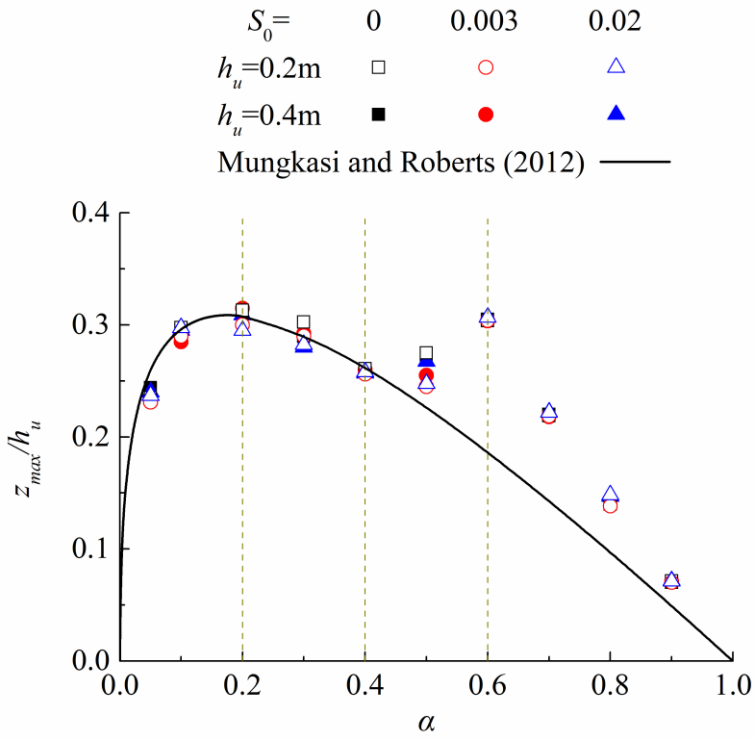

Fig. 21. Dimensionless wave-front height for different α and bed slopes.

3.6.2. First extra negative waves

Fig. 22 shows that the peak water level of the first extra negative wave decreases with the time. For flat and mild bed slope (e.g. S_0 = 0 and 0.003), the peak water level remains almost constant for a period of time and then falls down. For S_0 = 0.02, the peak water level is always falling and the change process of water level shows a gradual decrease followed by a sharp decline. It is maybe due to the fall of the water level at the end of the reservoir, which accelerates the peak water level of the first extra negative wave descending. This means that the extra negative waves formed in the limited-length reservoir will continue to dissipate during the propagation towards the reservoir area

in a relatively large bed slope. As such, the impact on the upstream structure will gradually decrease with the evolution of the flow.

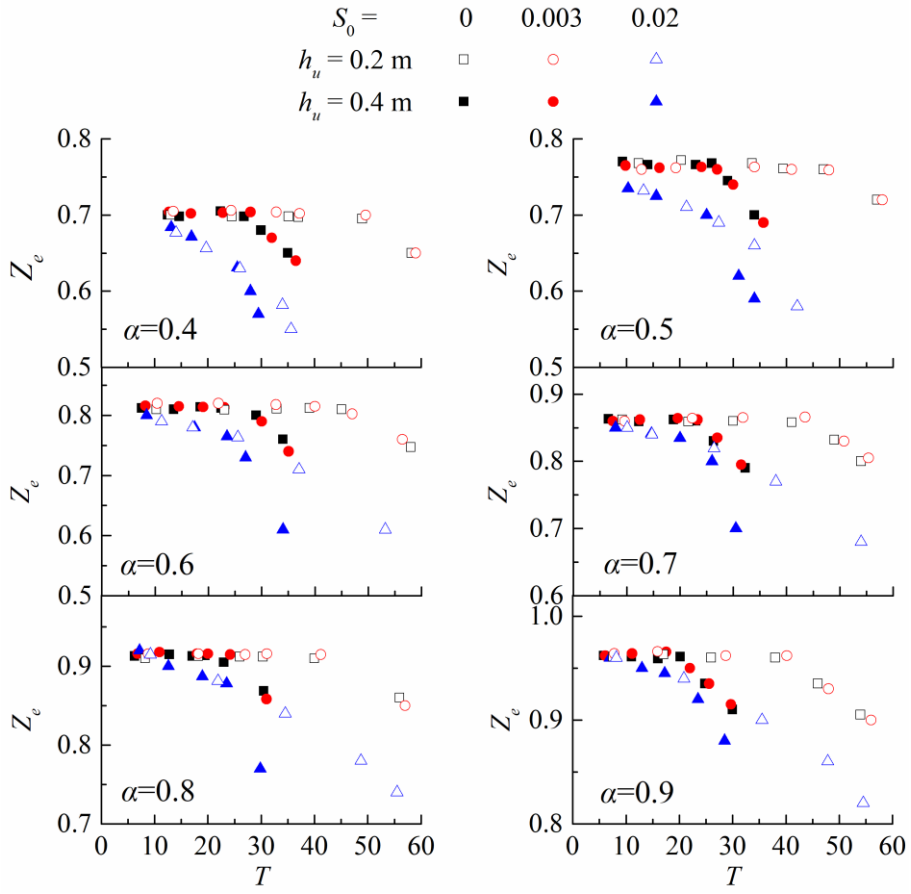

Fig. 22. Variation of peak level for the first extra negative wave.

4. Conclusions

In this paper, the experiments are carried out in a large flume under different bed slopes and downstream tailwater depths. The main conclusions are as follows:

(1)The experimental observation shows that the increase of the bed slope will change the evolution pattern of the dam-break flow. In the case of S_0 = 0 and 0.003, there are periodic waves (i.e. the extra negative waves) propagating towards the reservoir area when $\alpha \geq 0.3$, while Favre waves stably evolve downstream when $\alpha \geq 0.6$. The stable Favre waves can be formed in large water depth ration for steep slope (i.e. $\alpha \geq 0.5$, S_0 = 0.02 in this study). Increase of the bed slope makes *Fr* tend to

decline with time.

(2) The wave-front height shows a double-peak property with the α increases. The maximum wave-front height appears roughly when α = 0.2 for all three different bed slopes, and the dimensionless height is approximately 0.31. The first downstream wave causes the second maximum value to occur when α = 0.6. The wave-front height gradually decreases with the α increases when $\alpha \geq 0.6$. Since the wave-front height calculated based on the shallow water assumption is significantly small for $\alpha \geq 0.5$, it is more appropriate to use the calculation method which assumes a weak non-hydrostatic flow to descript the wave-front height (Soares-Frazao and Zech, 2002).

(3) The appearance of extra negative waves leads to a significant undulation of the water surface profiles and mean velocity in the reservoir. The frequency of the undulation gradually increases with the increase of α. The peak water level of the first extra negative wave is gradually falling after maintaining a stability value for a period of time when S_0 = 0 and 0.003, while it is always falling when S_0 = 0.02. Since the extra negative wave can affect the upstream channel, it needs to be considered in the design of the structure of the channel.

(4)The comparison with the analytical solutions shows that the negative wave celerity is better predicted by Dressler (1958), while the analytical solution of Chanson (2009) can better capture the motion of the wave-front. For small bed slope and water depth ration (i.e. S_0 = 0.003, $0 < \alpha < 0.3$), the analytical model of Mungkasi and Roberts (2012) can provide the relatively good prediction for the motion of flow. However, it cannot describe the periodic wave phenomenon that occurs in the reservoir area or downstream of the dam when $\alpha \geq 0.3$. For large bed slope S_0 = 0.02, the initial conditions assumed in the analytical solution of Mungkasi and Roberts (2012) are different from the experimental conditions, therefore, it is unable to use to predict the dam-break flow with steep slope.

The current research expands the understanding of the effects of the bed slope and the tailwater level on the movement of dam-break flows. The tailwater level and bed slope both have a significant impact on the evolution pattern of the dam-break flows. The Favre waves will apparently raise the

downstream water level in flood control. It is indicated that the water depth ratio is an important element when making flood emergency plans in real life.

Declaration of Competing Interest

None.

Acknowledgements

This study is supported by the National Natural Science Foundation of China (Grant No: 51879179), the Open Fund from the State Key Laboratory of Hydraulics and Mountain River Engineering, Sichuan University (SKHL1809) and Sichuan Science and Technology Program (No. 2019JDTD0007). Thanks to Liu Xin, Yang Sha, and Zhang Fengjie for their help in the experiment. Comments made by reviewers have greatly improved the quality of the final paper.

Notation

The following symbols are used in this paper:

b = flume width;

c = wave celerity;

c_{en} = first extra negative wave celerity;

c_{es} = first downstream wave celerity;

c_n = negative wave celerity;

c_w = wave-front celerity;

C = dimensionless wave celerity;

C_{en} = dimensionless first extra negative wave celerity;

C_{es} = dimensionless first downstream wave celerity;

C_n = dimensionless negative wave celerity;

548 C_w = dimensionless wave-front celerity;

549 Fr = Froude number;

550 g = gravity acceleration;

551 h = flow depth;

552 h_u = initial upstream water depth;

553 h_d = initial downstream water depth;

554 k_s = surface roughness height;

555 R^2 = correlation coefficient;

556 S_0 = bed slope;

557 t = time;

558 T = dimensionless time;

559 u = mean velocity;

560 $u_{(t)}$ = mean velocity at time t;

561 U = dimensionless mean velocity;

562 W = water volume;

563 $W_{(t)}$ = water volume at time t;

564 $W_{(t+\Delta t)}$ = water volume at time $t+\Delta t$;

565 x = distance along flow direction originated from dam site;

566 z = water level;

567 Z = dimensionless water level;

568 Δt = time space;

569 α = water depth ratio;

570

571 **References**

572 Bento, A.M., Amaral, S.V.T., Cardoso, R., Ferreira, R.M.L., 2017. Direct estimate of the breach

573 hydrograph of an overtopped earth dam. ASCE J. Hydraul. Eng. 143(6), 06017004.
574 https://doi.org/10.1061/(ASCE)HY.1943-7900.0001294.
575 Bishnu H., Devkota, Joerg I., 2009. Lagrangian modeling of weakly nonlinear nonhydrostatic
576 shallow water waves in open channels. J. Hydraul. Eng. 135(11), 926-934.
577 https://doi.org/10.1061/(ASCE)0733-9429(2009)135:11(926).
578 Cestero, J.A.F., Imran, J., Chaudhry, M.H., 2014. Experimental investigation of the effects of soil
579 properties on levee breach by overtopping. ASCE J. Hydraul. Eng. 141(4), 04014085.
580 https://doi.org/10.1061/(ASCE)HY.1943-7900.0000964.
581 Chanson, H., 2009. Application of the method of characteristics to the dam break wave problem.
582 J. Hydraul. Res. 47(1), 41-49. https://doi.org/10.3826/jhr.2009.2865.
583 Chen, H.Y., Xu, W.L., Deng, J., Xue, Y., Li, J., 2014. Experimental investigation of pressure load
584 exerted on a downstream dam by dam-break flows. ASCE J. Hydraul. Eng. 140(2), 199-207.
585 https://doi.org/10.1061/(ASCE)HY.1943-7900.0000743.
586 Cochard, S., Ancey, C., 2008. Tracking the free surface of time-dependent flows: image processing
587 for the dam-break problem. Exp. Fluids 44(1), 59-71. https://doi.org/10.1007/s00348-007-0374-3.
588 Denlinger, R.P., O'Connell, D.R., 2008. Computing nonhydrostatic shallow-flow over steep terrain.
589 ASCE J. Hydraul. Eng. 134(11), 1590-1602.
590 https://doi.org/10.1061/(ASCE)0733-9429(2008)134:11(1590).
591 Dressler, R.H. 1958. Unsteady non-linear waves in sloping channels, Proc. R. Soc. London Ser. A,
592 247, 186–198. https://doi.org/10.1098/rspa.1958.0177.
593 Favre H., 1935, 'Etude théorique et expérimentale des ondes de translation dans les canaux
594 découverts', Dunod, Paris.

595 Feizi, K.A., Tahershamsi, A., Soares-Frazao, S., 2012. Experimental investigation of reservoir
596 geometry effect on dam-break flows. J. Hydraul. Res. 50(4), 376-387.
597 https://doi.org/10.1080/00221686.2012.690974.
598 Fernandez-Feria, R., 2006. Dam-break flow for arbitrary slopes of the bottom. J. Eng. Math. 54(4),
599 319-331. https://doi.org/10.1007/s10665-006-9034-5.
600 Hamlet, A.F., Lettenmaier, D.P., 2007. Effects of 20th century warming and climate variability on
601 flood risk in the western u.s. Water Resour. Res. 43(6). https://doi.org/10.1029/2006WR005099.
602 Hooshyaripor, F., Tahershamsi, A., 2015. Effect of reservoir side slopes on dam-break flood waves.
603 Eng. Appl. Comp. Fluid, 9(1), 458-468. https://doi.org/10.1080/19942060.2015.1039630.
604 Hunt, B., 1983. Asymptotic solution for dam break on sloping channel. ASCE J. Hydraul. Eng.
605 109(12), 1698-1706. https://doi.org/10.1061/(ASCE)0733-9429(1983)109:12(1698).
606 Juez C., Soares-Frazao S., Murillo J., García-Navarro P., 2017. Experimental and numerical
607 simulation of bed load transport over steep slopes. J. Hydraul. Res. 55 (4), 455-469.
608 https://doi.org/10.1080/00221686.2017.1288417.
609 Kocaman, S., Ozmen-Cagatay, H., 2015. Investigation of dam-break induced shock waves impact on
610 a vertical wall. J. Hydrol. 525, 1–12. https://doi.org/10.1016/j.jhydrol.2015.03.040.
611 Lauber, G., Hager, W.H., 1998a. Experiments to dam break wave: horizontal channel. J. Hydraul. Res.
612 36 (3), 291–307. https://doi.org/10.1080/00221689809498620.
613 Lauber, G., Hager, W.H., 1998b. Experiments to dam break wave: sloping channel. J. Hydraul. Res.
614 36(5), 761-773. https://doi.org/10.1080/00221689809498601.
615 Liu, W.J., Wang, B., Chen, Y.L., Wu, C., Liu, X., 2018. Assessing the analytical solution of
616 one-dimensional gravity wave model equations using dam-break experimental measurements.

Water, 10 (9), 1261. http://www.mdpi.com/2073-4441/10/9/1261.

Liu, W.J., Wang, B., Zhang, J.M., Chen, Y.L., Wu, C., Liu, X., Song, J.J., 2019a. Experimental study on dam-break flows under different upstream and downstream initial water depth. Adv. Eng. Sci. 51 (2), 121–129. (in Chinese). https://doi.org/10.15961/j.jsuese.201800374.

Liu, X., Wang, B., Zhang, J.M., Chen, Y.L., Wu, C., Liu, W.J., Song, J.J., 2019b. A nonintrusive measurement of full-field water depth and its application in experimental investigations of dam-break flows. Adv. Eng. Sci. 51 (3), 52–58. (in Chinese). https://doi.org/10.15961/j.jsuese.201800689.

Mangeney, A., Heinrich, P., Roche, R., 2000. Analytical solution for testing debris avalanche numerical models. Pure Appl. Geophys. 157(6), 1081-1096. https://doi.org/10.1007/s000240050018.

Marche C, Beauchemin P. EL Kayloubi A., 1995. Etude numérique et expérimentale des ondes secondaires de Favre consécutives a la rupture d'un harrage, Can. J. Civil Eng., 22, 793-801. https://doi.org/10.1139/l95-089.

Marra, D., Earl, T., Ancey, C., 2011. Experimental investigations of dam break flows down an inclined channel. Proceedings of the 34th World Congress of the International Association for Hydro-Environment Research and Engineering: 33rd Hydrology and Water Resources Symposium and 10th Conference on Hydraulics in Water Engineering. Brisbane, Australia, 2011.

Melis, M., Poggi, D., Fasanella, G.O.D., Cordero, S., Katul, G.G., 2019. Resistance to flow on a sloping channel covered by dense vegetation following a dam break. Water Resour. Res. 55(2), 1040–1058. http://doi.org/10.1029/2018WR023889.

Miller, S., Chaudhry, M.H., 1989. Dam-break flows in curved channel. ASCE J. Hydraul. Eng.

115(11), 1465-1478. https://doi.org/10.1061/(ASCE)0733-9429(1989)115:11(1465).

Mungkasi, S., Roberts, S.G., 2011. A new analytical solution for testing debris avalanche numerical models. Anziam J. 52(CTAC2010): C349–C363. https://doi.org/10.21914/anziamj.v52i0.3785.

Mungkasi, S., Roberts, S.G., 2012. Analytical solutions involving shock waves for testing debris avalanche numerical models. Pure and Applied Geophysics, 169(10), 1847-1858. https://doi.org/10.1007/s00024-011-0449-1.

Nsom, B., Debiane, K., Piau, J.M., 2000. Bed slope effect on the dam break problem. J. Hydraul. Res. 38(6), 459-464. https://doi.org/10.1080/00221680009498299.

Peregrine, D., H., 1966. Calculations of the development of an undular bore. J. Fluid Mech. 25(02), 321. https://doi.org/ 10.1017/S0022112066001678.

Plate, E.J., 2005. Flood risk and flood management. J. Hydrol. 267(1), 2-11. https://doi.org/10.1016/S0022-1694(02)00135-X.

Sandover, J.A., Zienkiewcz, O.C., 1957. Experiments on surge waves. Water Power, 9, 418-24.

Soares-Frazao S., Zech Y., 2002. Undular bores and secondary waves -Experiments and hybrid finite-volume modelling, J. Hydraul. Res. 40:1, 33-43. https://doi.org/10.1080/00221680209499871.

Stoker, J.J., 1957. Water waves: The mathematical theory with applica-tions. New York: Interscience.

Treske, A., 1994. Undular bores (favre-waves) in open channels - experimental studies. J. Hydraul. Res. 32(3), 355-370. https://doi.org/10.1080/00221689409498738.

Van E.S., Zech Y., Soares-Frazao S., 2014. Limitations of the shallow water assumptions for problems involving steep slopes: application to a dike overtopping test case. International Conference on Fluvial Hydraulics, River Flow 2014 (Lausanne, Switzerland). In: River Flow

2014 - Proceedings of the International Conference on Fluvial Hydraulics (ISBN 978-1-138-02674-2) https://doi.org/10.1201/b17133-222, pp.1669-1677.

Wang, B., Chen, Y.L., Wu, C., Dong, J.H., Ma, X., Song, J.J., 2016. A semi-analytical approach for predicting peak discharge of floods caused by embankment dam failures. Hydrol. Process. https://doi.org/10.1002/hyp.10896.

Wang, B., Chen, Y.L, Wu, C., Peng, Y., Ma, X., Song, J.J., 2017. Analytical solution of dam-break flood wave propagation in a dry sloped channel with an irregular-shaped cross-section. J. Hydro-environ. Res. 14, 93–104. https://doi.org/10.1016/j.jher.2016.11.003.

Wang, B., Chen, Y.L, Wu, C., Peng, Y., Song, J.J., Liu, W.J., Liu, X., 2018. Empirical and semi-analytical models for predicting peak outflows caused by embankment dam failures. J. Hydrol. 562, 692–702. https://doi.org/10.1016/j.jhydrol.2018.05.049.

Wang, B., Zhang, J.M., Chen, Y.L., Peng, Y., Liu, X., Liu, W.J., 2019. Comparison of measured dam-break flood waves in triangular and rectangular channels. J. Hydrol. 575(2019), 690-703. https://doi.org/10.1016/j.jhydrol.2019.05.081.

Wang, B., Liu, W.J., Zhang, J.M., Chen, Y.L., Wu, C., Peng, Y., Wu Z.Y., Liu, X., Yang, S., 2020a. Enhancement of semi-theoretical models for predicting peak discharges in breached embankment dams. Environ Fluid Mech. https://doi.org/10.1007/s10652-019-09730-9.

Wang, B., Chen, Y.L., Peng, Y., Zhang, J.M., Guo, Y.K., 2020b. Analytical solution of shallow water equations for ideal dam-break flood along a wet bed slope. ASCE J. Hydraul. Eng. 146(2), 06019020. https://doi.org/10.1061/(ASCE)HY.1943-7900.0001683.

Wang, B., Liu, X., Zhang, J.M., Guo, Y.K., Chen, Y.L., Peng, Y., Liu, W.J., Yang, S., Zhang, F.J., 2020c. Analytical and experimental investigations of dam-break flows in triangular channels with

683 wet-bed conditions. ASCE J. Hydraul. Eng. Accepted.
684 https://doi.org/10.1061/(ASCE)HY.1943-7900.0001808.
685 Wang, B., Liu, W.J., Wang, W., Zhang, J.M., Chen, Y.L., Peng, Y., Liu, X., Yang, S., 2020d.
686 Experimental and numerical investigations of similarity for dam-break flows on wet bed. J.
687 Hydrol. 583(2020)124598. https://doi.org/10.1016/j.jhydrol.2020.124598.
688 Wang, L.H., Pan, C.H., 2014. An analysis of dam-break flows on slope. J. Hydrodyn. 26(6), 902-911.
689 https://doi.org/10.1016/S1001-6058(14)60099-8.
690 Wood, A., Wang, K.H., 2015. Modeling dam-break flows in channels with 90 degree bend using an
691 alternating-direction implicit based curvilinear hydrodynamic solver. Comput. Fluids, 114,
692 254-264. https://doi.org/10.1016/j.compfluid.2015.03.011.
693

694 **Tab. captions list**

695 Tab. 1. Experimental parameters.

696

697 **Fig. captions list**

698 Fig. 1. Sketch of the flume device.

699 Fig. 2. Evolution pattern of the dam-break flows at t = 0.42 s (a) S_0 = 0; (b) S_0 = 0.003; (c) S_0 = 0.02.

700 Fig. 3. Evolution pattern of the dam-break flows at t = 3.54 s (a) S_0 = 0; (b) S_0 = 0.003; (c) S_0 = 0.02.

701 Fig. 4. Characteristics of the Favre waves under different bed slopes.

702 Fig. 5. Generalized model when waves appear upstream and downstream.

703 Fig. 6. Dimensionless free surface profiles for α = 0.

704 Fig. 7. Dimensionless free surface profiles for α = 0.1.

705 Fig. 8. Dimensionless free surface profiles for (a) α = 0.3; (b) α = 0.5; (c) α = 0.7.

706 Fig. 9. Stage hydrographs for α = 0 (a) reservoir area; (b) downstream of the dam.